Advanced Microwave Ferrite Research (AMFeR):
Phase Two

A Final Report Submitted
to

Dr. Colin Wood
Office of Naval Research
Code 312, Electronics Division
One Liberty Center
875 North Randolph Street, Suite 1425
Arlington, VA 22203-1995
703-696-4218
woodc@onr.navy.mil

by

Dr. Jeffrey L. Young
MRC Institute/Electrical and Computer Engineering
University of Idaho
Moscow, ID 83844-1024
208-885-6829
jyoung@mrc.uidaho.edu

on

December 31, 2006

Supporting Information:

Contract Number: N00014-05-1-0239

Original Contract Period: February 15, 2005 through March 30, 2006
Extended Contract Period: April 1, 2005 through December 31, 2006

FY05 Funded Amount: $1,053,000

Executive Summary:

Reported herein are the key findings and activities associated with the Office of Naval Research (ONR) Advance Microwave Ferrite Research (AMFeR) Phase Two project. This project was conceived to develop high anisotropy ferrite crystals for microwave, self-biased circulator devices. To accomplish the research objectives stated in the proposal to ONR, the AMFeR team organized itself into three task-oriented groups: material fabrication, micromagnetic modeling and microwave device design. Principle team members of the material fabrication group included Profs. Y.-K. Hong, D. McIlroy, and W. J. Yeh. Prof. R. Wells led the effort in micromagnetic modeling; Prof. J. Young was the principle project director and group leader for the microwave device group.

To date, barium-ferrite, c-axis crystals have been grown using several methods, including sputtering and liquid phase epitaxy, with the latter method being the most successful for the growth of thick crystals in excess of 100 microns. The crystals were characterized using a variety of apparatuses including a vibrating sample magnetometer (VSM), x-ray diffractometer (XRD), single crystal x-ray diffractometer, scanning electron microscopy (SEM), optical microscopy, and magnetic force microscopy (MFM). Anisotropy fields and saturation magnetization were found via measurement to be in the range of 10 to 18 kOe and 4.0 to 4.6 G, respectively; both of these ranges are consistent with other findings found in the literature.

Micromagnetic simulations were carried out for various experimental films developed by the materials team. Simulations of magnetic domain wall motion for the single crystal LPE films were a qualitative success, but a complete set of parameters for these films has not yet been achieved. Key discoveries associated with this endeavor included the need to 1) use a free energy expression that includes both uniaxial and direction-cosine terms and 2) introduce a thermal energy term using a stochastic Landau-Lifshitz equation. These terms were shown to yield simulation data that agreed quite well with the measured longitudinal-plane and normal-plane hysteresis and torque curve data. Since the micromagnetic modeling effort has reach maturation as far as the AMFeR project is concerned, this activity will play a minor role in future phases of the project.

The microwave device team continued its investigation of the design of novel shaped ferrite microwave circulator and ferrite front-end microwave assemblies. Several microwave circulators were designed that achieved good isolation and bandwidth characteristics. For example, a fabricated square ferrite circulator achieved about 14 dB of isolation over a 2 GHz bandwidth centered about 10 GHz. The group also developed high precision circulator models for its design optimization routines and devised a technique to determine the impact of material loss mechanisms on circulator performance. To further enhance the experimental capabilities of the group, the construction of a new 2-40 GHz anechoic chamber was initiated and the development of a microwave ferromagnetic linewidth measurement apparatus was built in collaboration with Colorado State University (Prof. Carl Patton, sub-investigator). The system can be configured to

measure linewidth using either a shorted waveguide or a high-Q cavity in swept field or swept frequency mode.

A more comprehensive report on the aforementioned activities can be found in Appendices A through E, which have been prepared by each team member. The appendices are organized alphabetically by author as follows:

- Appendix A: Y. K. Hong, "Development of Hexaferrite Thick Films by Sputtering and Liquid Phase Epitaxial Processes"
- Appendix B: D. N. McIlroy and W. J. Yeh, "Film Fabrication using Liquid Epitaxy Reflow Method"
- Appendix C: C. F. Patton and Nan Mo, "FMR Linewidth Measurements"
- Appendix D: R. Wells, "Micromagnetic Modeling"
- Appendix E: J. L. Young, "Microwave Circulator Design"

AMFeR Advisory Board

In September of 2005 the AMFeR team met with an informal advisory board and other visitors on the Moscow campus to discuss research accomplishments and directions. The meeting was well attended by experts from academia, governmental laboratories and industry. Those in attendance included Dr. Ralph Simmons (Hewlett-Packard Corporation), Dr. Harvey Newman (Navy Research Laboratory), Dr. Mohammad Mojarradi (NASA Jet Propulsion Laboratory), Dr. Carl Patton (Colorado State University), Mr. Nan Mo (Colorado State University), Dr. Denis Webb (consultant and former employee of the Naval Research Laboratory), and Mr. Stanley Gaglione (Northrop Grumman).

Future Work:

Both the material processes and laboratories are in place to commence with the fabrication of actual self-biased circulators. During Phase Three, attempts will be made to deposit c-axis, barium ferrite material within a circular aperture of some host dielectric. This deposition has been tested to some extent during Phase II and preliminary findings point to a successful outcome during Phase III. In this case success is construed to mean deposited ferrite material that exhibits good c-axis orientation, magnetic saturation, coercivity, linewidth and squareness. Once the ferrite material has been deposited in the host dielectric, copper traces will be patterned on the dielectric/ferrite substrate per the design requirements of the circulator. Scattering parameters will then be measured to determine the circulator's port response and matching networks will be suitably designed to create the necessary impedances for good circulation.

Journal Publications:

Y. Kranov, A. Abuzir, T. Prakash, D. N. McIlroy, and W. J. Yeh, "Barium hexaferrite thick films made by liquid phase epitaxy reflow method," *IEEE Transactions on Magetics* (Accepted for publication).

C. C. Juan, Y. K. Hong, S. H. Gee, I. T. Nam, J. Jalli, B. Mackowiak, C. Weatherspoon, and A. Lyle, "Barium ferrite films with negative nucleation field for self-biased circulator applications," *IEEE Transaction Magnetics* (Submitted).

S. H. Gee, Y. K. Hong, I. T. Nam, C. Weatherspoon, A. Lyle, and J. C. Sur, "$Ba_3Co_{0.8}Zn_{1.2}Fe_{24}O41$ (Co_2Z-type) hexa-ferrite particles for LTCC substrates," *IEEE Transaction on Magnetics* (Accepted for publication).

J.L. Young, R.S. Adams, B. O'Neil, and C.M. Johnson, "Bandwidth optimization of an integrated microstrip circulator and antenna assembly: Part Two," *IEEE Antennas and Propagation Magazine*, (Accepted for publication, February 2007)

J.L. Young, R.S. Adams, B. O'Neil, and C.M. Johnson, "Bandwidth optimization of an integrated microstrip circulator and antenna assembly: Part One," *IEEE Antennas and Propagation Magazine*, (Accepted for publication, December 2006)

Conference presentations:

W. J. Yeh, J. Krehbiel, and A. R. Abuzir, "Comparative study of the magnetic properties of Ba-Ferrite thin films deposited on different substrates," American Physical Society, Baltimore, Maryland, March 2006.

A. Abuzir and W. Y. Yeh, "Barium hexaferrite made by liquid phase epitaxy reflow method," Eighth Annual Meeting of the American Physical Society Northwest Section, Tacoma, Washington, May, 2006.

A. Abuzir, Y. Kranov, T. Prakash, D. McIlroy and W. Y. Yeh, "Barium hexaferrite made by liquid phase epitaxy reflow method," International Magnetics Conference, San Diego, California, May 2006.

C. C. Juan, Y. K. Hong, S. H. Gee, and J. Jalli, "Barium ferrite thin films with negative nucleation field for self-biased circulator applications," IEEE International Magnetics Conference, San Diego, California, May 2006.

S. H. Gee, Y. K. Hong, J. C. Sur, and C. Weatherspoon, "$Ba_3Co_{2-x}Co_xZn_xFe_{24}O_{41}$ ferrites processed by mechanical alloying for LTCC," IEEE International Magnetics Conference, San Diego, California, May 2006.

R.S. Adams and J.L. Young, "Integration of a microstrip circulator and antenna assembly," IEEE Antennas and Propagation International Symposium and USNC/URSI National Radio Science Meeting, Albuquerque, New Mexico, July 2006.

Theses and Dissertations:

Ryan Adams, "Bandwidth optimization of an integrated microstrip circulator and antenna assembly," Master of Science, Electrical Engineering, (Jeffrey L. Young, Advisor), October 2005.

Feng Xie, "A micromagnetic model of barium ferrites for microwave circulator design," Doctor of Philosophy, Electrical Engineering, (Richard Wells, Advisor), June 2006.

Patents:

Y. K. Hong, S. H. Gee, J. Jalli, C. C. Juan, and B. Marckowiak, "Liquid phase epitaxial (LPE) growing process for barium ferrite (BaM: $BaFe_{12}O_{19}$) 100 micron thick films on sapphire (Al_2O_3) single crystal substrates for high frequency circulators" (Disclosed to the Idaho Research Foundation, August 22, 2005).

J. L. Young, R. S. Adams, B. O'Neil, "Integrated Microstrip Circulator and Microwave Device Assembly," (Patent filed in August 2006).

Funded Graduate Research Assistants:

- Alaaedeen Abuzir
- Ryan Adams
- Sung-Hoon Gee
- C. C. Juan
- Jeevan Prasad Jalli
- Benton O'Neil
- Yanko Kranov
- Jonathon Watkins
- Feng Xie

Funded Undergraduate Research Assistants:

- Marcus Sky Driver
- Justin Lantrip
- Brady Machowiak
- Andrew Ulrich
- C. Weatherspoon

Miscellaneous:

Yang-Ki Hong, Member, IEEE 2006 International Magnetics Conference Program Committee, San Diego, California, May 2006.

J. L. Young, Session Co-Chair (with D. Anagnostou), "Planar Passive Devices," IEEE Antennas and Propagation International Symposium and URSI Radio Science Meeting, Albuquerque, New Mexico, 2006.

J. L. Young, Member, Technical Program Committee, IEEE International Symposium on Antennas and Propagation and USNC/URSI Radio Science Meeting, Albuquerque, New Mexico, 2006.

J. L. Young, Judge, Student Paper Competition, IEEE Antennas and Propagation International Symposium and URSI Radio Science Meeting, Albuquerque, New Mexico, 2006.

J. L. Young, Associate Project Director, Defense Experimental Program to Stimulate Competitive Research for the State of Idaho, 2006-present.

Appendix A

Development of Hexa-ferrite Thick Films by Sputtering and Liquid Phase Epitaxial Processes

Yang-Ki Hong

I. Abstract

The principle objective of this research project is to develop thick hexa-ferrite ($BaFe_{12}O_{19}$; BaM) films and single crystals for self-biased microwave circulators operating in the range of 35 GHz and above. The approach to accomplish this objective primarily consists of employing the following techniques

a) Liquid phase epitaxy (LPE) process to grow thick (> 100μm) BaM films.
b) High temperature/slow furnace cooling to grow bulk BaM single crystals.
c) Sputter deposition technique to deposit bi-layer BaM film having a negative nucleation field.
d) Solid-stated reaction process to synthesis magneto-dielectric ($Ba_3Co_{0.8}Zn_{1.2}Fe_{24}O_{41}$)Z-type hexa-ferrite ($Co_{0.8}Zn_{1.2}Z$) for low temperature co-fired ceramics (LTCC) substrates.

High quality thick BaM films (greater than 100 μm) and bulk single crystals (3mm x 4mm x 0.7mm) were successfully grown. Anisotropy field (H_k) of BaM Bulk single crystals were controlled by cation substitution for Fe^{3+} sites of BaM crystal. Substituted cations include Mn, Al, Zr, Sn, and Co. In order to achieve self-biasing nature in BaM films, we developed polycrystalline BaM thin films that possess a negative nucleation field. In addition, magneto-dielectric ($Ba_3Co_{0.8}Zn_{1.2}Fe_{24}O_{41}$) Z-type hexa-ferrite ($Co_{0.8}Zn_{1.2}Z$) was synthesized for microwave devices and miniature antennae in the 1 – 2 GHz range.

Vibrating sample magnetometer (VSM), x-ray diffractometer (XRD), single crystal x-ray diffractometer, scanning electron microscopy (SEM), optical microscopy, magnetic force microscopy (MFM), and network analyzer were used to characterize the physical and magnetic properties of the film, bulk single crystals and $Co_{0.8}Zn_{1.2}Z$ particles. The crystallographic BaM thick film was confirmed by analysis of single crystal x-ray diffractometer. SEM and optical microscopy study of BaM thick film morphologies suggested a layer growth mechanism in which slabs of crystal grow predominantly by edge addition of atoms and self-overlapping.

Anisotropy field (H_k) and saturation magnetization ($4\pi M_s$) of BaM single crystal film/bulk with dopants were found to be in the range of 10 to 17.80 kOe and 4 to 4.56 kG, which are very close to the bulk values reported in the literature. The polycrystalline 0.2 μm thick BaM films developed by *ex-situ* annealing process possesses a negative nucleation field of -1.6 kOe and squareness of 0.95. Characterizations of microwave properties are in progress for both thick films and the bulk single crystal samples.

II. Proposal Objectives:

Oriented hexagonal hexa-ferrite (BaM) has been used as potential candidates for various microwave devices in the millimeter wavelength range for the past several decades. BaM possesses a high uniaxial anisotropy field, which can allow one to develop self-biased microwave devices such as circulators and isolators operating in the GHz range without any external biasing field. The large uniaxial anisotropy field of BaM with a positive anisotropy constant acts like an externally applied field. Large resistivity, high permeability, narrow magnetic anisotropy field distribution, and chemical stability of BaM have stimulated researchers towards miniaturized thick-film development for circulators and isolators operating at millimeter wave frequencies.

In the past microwave devices such as circulators and phase shifter are constructed using bulky external magnets or electromagnets to maintain and control the ferrite magnetization for achieving a low loss tangent at high operating frequencies. To produce self-biased magnetic thick films for the application to the final device at the microwave frequencies the thick films need to be more than 100 μm with a *c*-axis orientation and a negative nucleation field (H_N), which compensates for the demagnetization field. Additionally, high squareness (SQ = M_r/M_s) is required to maintain high magnetic flux in circulator operation and eliminates the need for an external biasing field. In order to address these issues, we investigated and optimized a new LPE flux system to grow high quality thick films and bulk single crystals. High temperature/slow cooling furnace process was also employed to further investigate the change in anisotropy with different cation substitutions into the single crystal BaM system. Polycrystalline BaM film with negative nucleation field was developed to introduce the self-biasing nature in BaM films by an optimized *ex-situ* annealing process. However, this achievement is currently in the process of study for a plausible application for self-biased circulators.

III. Methodology:

BaM thick film and bulk single crystal growth by LPE process

$BaFe_{12}O_{19}$ flux melt was prepared from a mixture of iron oxide (Fe_2O_3), barium carbonate ($BaCO_3$), and sodium carbonate (Na_2CO_3). The powders were ground and mixed homogeneously and calcinated at an elevated temperature for 12 hours. After the process of calcination, the starting materials are fed in a Pt crucible and heated initially to melt in an rf induction furnace. The priority melt in Pt crucible was subjected to the LPE system at room temperature, where it was again heated to a temperature of 1250 °C. The temperature of the furnace was cooled slowly to the growth temperature prior to dipping the 0.5 μm thick BaM seed layer deposited on to (000*l*) α-Al_2O_3 substrate. The substrate was then lowered into the melt to grow thick BaM film. Bulk single crystals are formed in the melt during the process of homogenization and cooling, these crystals are carefully collected at the end of the LPE process by leaching process at room temperature.

Cation substituted BaM single crystals by high temperature/slow furnace cooling process

High purity BaM single crystals were grown with the substitutions of different divalent elements of Mn, Al, Zr, Sn, and Co by using a high temperature/slow cooling furnace. The single crystals were grown from the melts without using any seed crystals or addition of any flux systems. The primary mixtures of $BaCO_3$, α-Fe_2O_3 with small additions of the respective doping elements were used to obtain the desired BaM single crystals of $BaFe_{11.6}Co_{0.2}Sn_{0.2}O_{19}$, $BaFe_{11.6}Al_{0.2}Mn_{0.2}O_{19}$, $BaFe_{11.6}Co_{0.2}Zr_{0.2}O_{19}$, and $BaFe_{11.8}Mn_{0.2}O_{19}$. The well mixed primary reagents were ground together in a mortar with pestle for 1 hour thoroughly and then filled in a Pt crucible. The Pt crucible was subjected to a top-lift enclosed high temperature furnace and fired at the temperature of 1650 °C for 2 hours to homogenize the melt. After completely homogenizing the melt, the crucible was slowly cooled down to 900 °C and later furnace cooled to room temperature.

The detail compositions of each constituent for growing the single crystals are summarized in Table I.

Table I. Composition in grams of the cations substituted BaM single crystal

Component	$BaCO_3$	Fe_2O_3	MgO	SnO_2	ZrO_2	Co_3O_4	Al_2O_3	MnO
$BaFe_{11.6}Co_{0.2}Sn_{0.2}O_{19}$	9.6	46.4	-	1.5	-	0.74	-	-
$BaFe_{11.6}Al_{0.2}Mn_{0.2}O_{19}$	9.6	46.4	-	-	-	-	0.58	0.4
$BaFe_{11.6}Co_{0.2}Zr_{0.2}O_{19}$	9.6	46.4	-	-	1.23	2.41	-	-
$BaFe_{11.8}Mn_{0.2}O_{19}$	9.6	46.4	-	-	-	-	-	0.4

Polycrystalline bi-layer BaM film with negative nucleation field

Bi-layer BaM film was deposited by using an rf sputtering system with a base pressure of 5 x 10^{-7} torr. The working pressure was maintained at 5 mtorr with a gas mixture of Ar-20 % O_2. The applied power was 2 W/cm^2. The (000*l*) α-Al_2O_3 single crystal sapphire substrates were chosen because of the 7 % lattice mismatch between BaM and α-Al_2O_3 substrate basal planes, and oxide substrates can withstand the high temperatures required for *ex-situ* annealing.

The bi-layer film was composed of a bottom crystalline BaM layer and a top Ba-Fe-O layer deposited under the same sputtering conditions, but with different heat-treatment conditions. The 0.1 μm thick bottom and top layers were deposited on the substrate at 950 °C and at room temperature, respectively. A total thickness of 0.2 μm resulted for the bi-layered BaM film. A series of *ex-situ* heat-treatment steps were further employed to crystallize the top Ba-Fe-O layer. Heat-treatment procedures were done with a rapid thermal annealing (RTA) system: first, at 900 °C for 1 min., second, 1000 °C for 5 min., and finally, at 1100 °C for 3 min., sequentially.

$Ba_3Co_{0.8}Zn_{12}Fe_{24}O_{41}$ hexa-ferrite particles for LTCC Substrates

Starting materials for the synthesis of $Co_{0.8}Zn_{1.2}Z$ nanoparticles were $BaCO_3$, CoO, ZnO, and 40 nm sized α-Fe_2O_3 particles according to their mole ratios with the composition. To prepare the nanoparticles the primary mixtures of the starting materials were shake-milled for 20 h with hardened-steel balls in a jar. The shake-milled particles were heat-treated in air at 1350 °C for 6 hours. The heat-treated powder was later subjected to shake-milling to improve the homogeneity of the heat-treated powder and to increase the surface area of the particles. After shake-milling, the powder was re-heat-treated at 1350 °C for 6 h either in an oxygen environment or in air. In order to prepare sintered disks, the heat treated or oxygen-heat-treated $Co_{0.8}Zn_{1.2}Z$ powder was mixed with the sintering agent Bi_2O_3 and pressed in a steel mold. Green disks (ϕ = 12.5 mm) and toroid (ϕ_{ID} = 3 mm, ϕ_{OD} = 7 mm) sample were then sintered in air at 900 °C for 6 h for identification of crystal phases and to characterization for magnetic properties.

Characterization

Physical and magnetic properties of the LPE processed BaM thick film with single crystals, cation substituted BaM single crystals, polycrystalline bi-layer BaM film, $Co_{0.8}Zn_{1.2}Z$ particles, and sintered disks were characterized by x-ray diffractometer (XRD), vibrating sample magnetometer (VSM) with a maximum applied field of 10 kOe, optical microscopy, scanning electron microscopy (SEM), atomic force microscopy (AFM), and magnetic force microscopy (MFM).

IV. Results

BaM thick film and BaM single crystal grown by LPE process

After one hour of LPE growth, the total thickness of barium ferrite (BaM) film on (000*l*) α-Al_2O_3 substrate was measured to be 107 μm by cross section morphology of SEM, which was reported in our Phase-I final report 2005, as shown in Fig. 1. The coercivity of the LPE processed thick BaM film was 3.6 Oe implying that the films has relatively small defects and voids. The saturation magnetization ($4\pi M_s$) and uniaxial magnetic anisotropy field (H_k) values for 107 μm film on α-Al_2O_3 substrate were 4.5 kG and 17

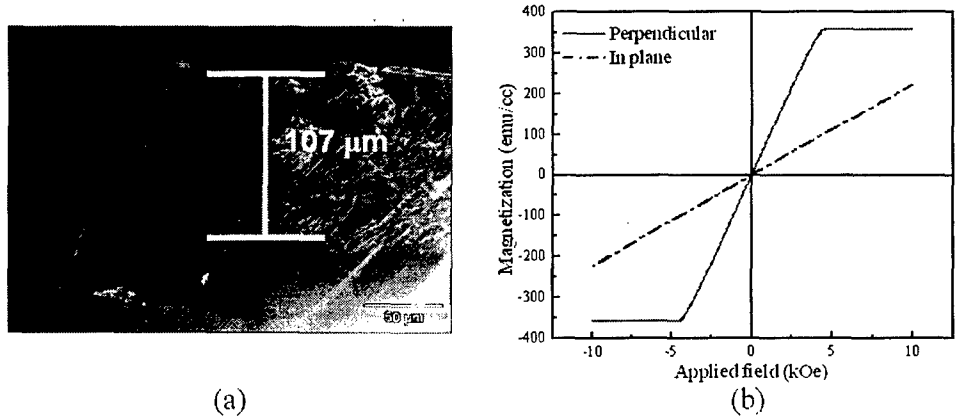

FIG. 1. (a) Scanning electron micrograph of a cross sectional area and (b) B-H loops of 107 μm thick LPE processed BaM film on (000*l*) α-Al_2O_3 substrate

kOe at room temperature, respectively. These values are close to those of bulk BaM properties reported in the literature.

To confirm the crystal structure and the orientation of the thick BaM films, a fragment of the BaM film was selected, attached to a glass fiber, and data was collected at 298(2) K using a Bruker/Siemens SMART APEX Single Crystal Diffraction instrument (MoK_α radiation, λ = 0.71073 Å). Data was measured using omega scans of 0.3 ° per frame for 10 seconds, and a full sphere of data was collected. A total of 2450 frames were collected with a final resolution of 0.71 Å. The first 50 frames were recollected at the end of the data collection in order to monitor for decay. Cell parameters were retrieved using SMART software and refined using SAINTPlus on all observed reflections. Data reduction and correction for Lp and decay were performed using the SAINTPlus software. Absorption corrections were applied using SADABS. The structure was solved by direct methods and refined by least squares method on F^2 using the SHELXTL program package. The structure was solved in the space group P6(3)/mmc (# 194) by analysis of systematic absences. All atoms were refined anisotropically. No decomposition was observed during data collection. Details of the data collection and refinement are given in Table II. The X- ray diffraction data confirmed that the structure is an extended single crystalline array with the composition $BaFe_{12}O_{19}$. The film crystallizes in the hexagonal space group P6(3)/mmc (Table II). Figure 2(a) shows a rotation photograph of the crystalline material and Fig. 2(b) displays a polyhedral representation of the structure of this compound. The structure closely matches the previously reported room temperature structure of $BaFe_{12}O_{19}$. The quality of the crystalline material is displayed by a very low final R = 0.0218 at 2θ = 30.06°. The films grew with the *c*-axis normal to the substrate plane.

Table II. Crystal data and refinement parameters for BaM

Formula	$BaFe_{12}O_{19}$
formula wt	1111.54
crystal system	Hexagonal
Space group	P6(3)/mmc
a (Å)	5.8926(3)
b (Å)	5.8926(3)
c (Å)	23.190(2
V (Å3)	697.34(8)
Z	2
T (K)	298(2)
λ (Å)	0.71073
ρ calc (Mg/m3)	5.294
μ (mm-1)	14.956
F(000)	1040
crystal size (mm3)	0.27 x 0.20 x 0.16
θ range(°)	1.76 to 30.06
Index ranges	$-8\leq h\leq 8$, $-8\leq k\leq 8$, $-31\leq l\leq 32$
Refl. Collected	10567
Indep. Reflections	445 [R(int) = 0.0326]
data/restraints/param.	445 / 0 / 42
GOF	1.000

*R1 [I>2σ (I)]	0.0218
*wR2 [I>2σ(I)]	0.0400
Largest diff. peak, hole (eÅ-3)	0.859,.-0.738

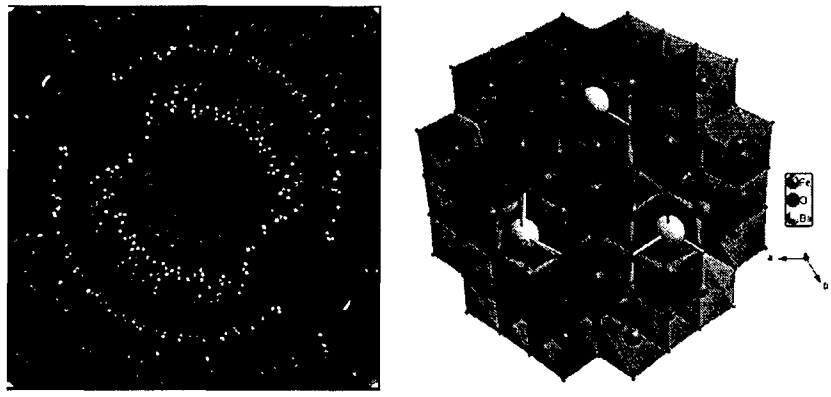

(a) (b)

FIG. 2. (a) Rotation (Oscillation) photograph of 107 μm thick LPE processed BaM film (b) polyhedral representation of the structure of BaM. Atoms types are indicated in the legend. View is down the

Torque magnetometry results confirm the excellent magnetic orientation of the BaM films. Figure 3 shows the magnetic torque versus rotation angle for 107 μm thick BaM film where the film is rotated both clockwise and counterclockwise around an axis in the film plane in an applied field of 10 kOe. A distinct uniaxial symmetry is apparent for both curves, where H lies normal to the film plane near 10° and 190°, and the difference between rotation directions is apparent at angles near the magnetically hard in-plane orientation since H has insufficient intensity to align the magnetization into the film hard plane. Measurements that are taken with H rotating in the film plane show no discernable variations in torque with the film in-plane angle, indicating that there is no preferential component of in-plane anisotropy.

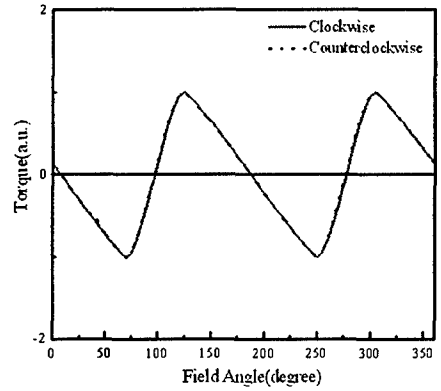

FIG. 3. Torque measurement of 107 μm thick LPE processed BaM film (at H_{App} = 10 kOe)

Optical micrograph in Fig. 4(a) shows the top view of bulk BaM single crystal collected from solid melt in the Pt crucible at room temperature after the LPE process. Most of the BaM single crystal had good layer morphologies on different scales, as shown in Fig. 4 (a). Figure 4(b) is an SEM picture take at 20 X magnification to show the spiral like geometry growing in the easy direction hexagonally. Figure 4(a) and 4(b) reveal some of the finer details of the layer structure of the crystal, showing the grooved leading edges. Figure 5(a) shows a polished surface of a BaM single crystal where the appearance is of sideways growing plates overlapping each other, and in several cases self-overlapping.

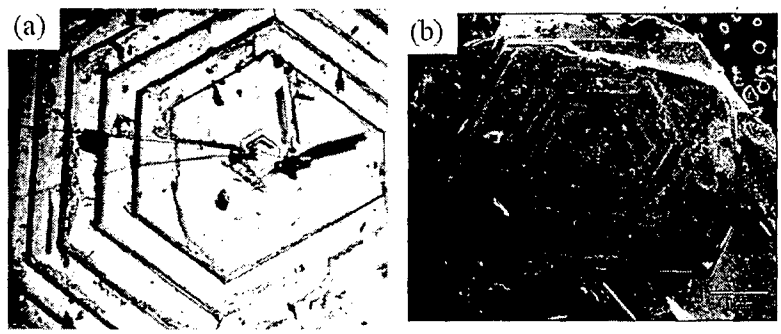

FIG. 4. (a) Optical micrograph and (b) scanning electron micrograph of the surface of a bulk BaM single crystal

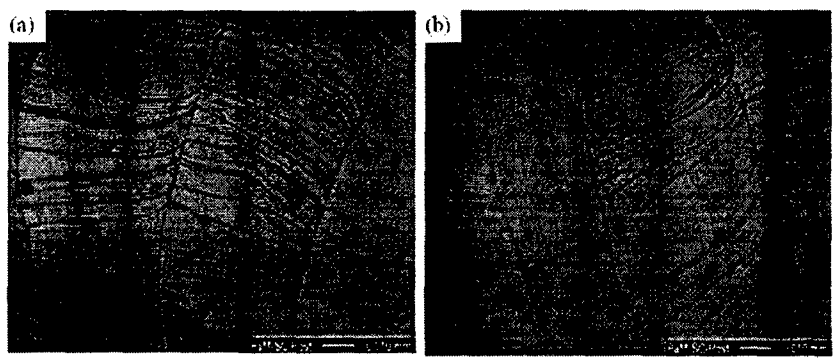

FIG. 5. Optical micrographs of a polished BaM single crystal surface (a) top view and (b) bottom view (the other side)

Figure 5(b) is another example at a later stage of growth suggesting a chaotic formative mechanism with plates and slabs growing sideways and overlapping.

MFM images were taken to study the magnetic domains of the fine polished BaM single crystal samples. Figure 6 shows the AFM and MFM images of the as-polished sample. Well-isolated, highly contrasting grains with lengths are observed. The isolation of the grains allowed correlating the grains to their magnetic domain structures. Most of the long grains showed regions of bright contrasts along one long edge and dark contrast along the other long edge in the MFM image. Bright or dark contrast indicates an

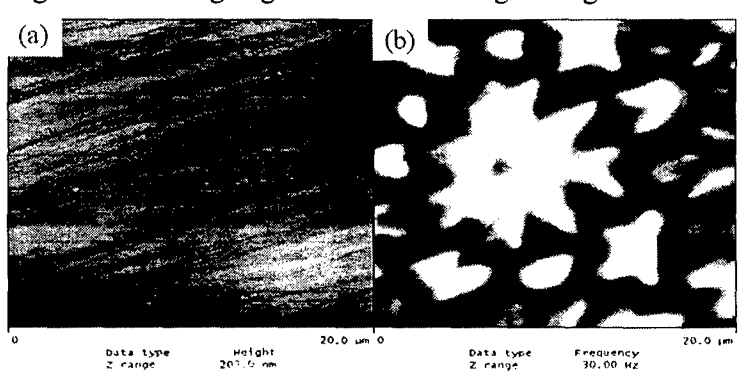

FIG. 6. (a) AFM and (b) MFM images of the as-polished BaM single crystal

upward or a downward vertical field gradient originating from the positive or negative magnetic charges respectively. Dark contrast along one edge and bright contrast along the other indicates an in-plane domain, with magnetization pointing from bright to dark contras-ting regions. Few grains, however, exhibited bright or dark contrast alternating along their elongated directions. This type of contrast indicates a perpendicularly oriented easy axis. Each bright or dark contrast corresponds to a perpendicular domain.

Cation substituted BaM single crystals by high temperature/slow furnace cooling process

The hysteresis loops in Fig. 7 show the magnetization curves of different samples measured in perpendicular direction of the cations substituted BaM single crystals. The saturation magnetization of Co-Zr substituted BaM single crystal increased to 68.6 emu/g from 68.0 emu/g but the uniaxial anisotropy decreased from 17 to 10 kOe. Saturation magnetization and uniaxial anisotropy field of Co-Sn, Al-Mn, and Mn substituted BaM single crystal are shown in Table III. The substitution of the iron ions by other cations leads to a strong asymmetry in the component due to the occupation of the cations in the preferential sites of $4f_{VI}$ by interrupting 12k-$4f_{VI}$ and $4f_{VI}$- $4f_{VI}$ superexchange interactions. As the substituted cation concentration increases in BaM, superexchange interactions become weak and second-order energy terms such as the antisymmetric interaction or magneto crystalline anisotropy start to play their role and non-colinear structures may appear.

Table III. Saturation magnetization and anisotropy field of cations substituted BaM single crystal

Component	Saturation magnetization (emu/g)	Anisotropy field (kOe)
$BaFe_{11.6}Co_{0.2}Sn_{0.2}O_{19}$	64	12.5
$BaFe_{11.6}Al_{0.2}Mn_{0.2}O_{19}$	63.9	17.8
$BaFe_{11.6}Co_{0.2}Zr_{0.2}O_{19}$	68.6	10.0
$BaFe_{11.8}Mn_{0.2}O_{19}$	60.2	14.5
$BaFe_{12}O_{19}$	68.0	17.0

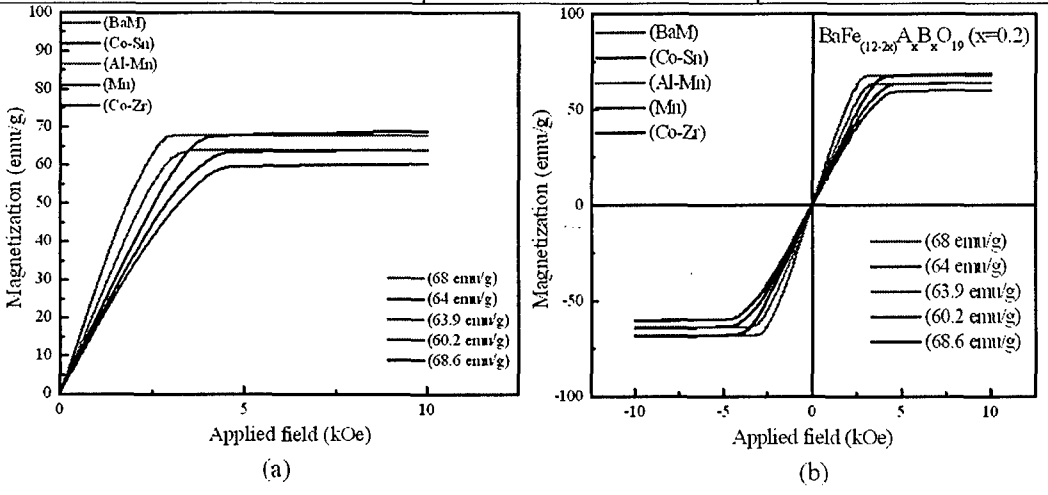

FIG. 7. B-H loops of different cations substituted BaM single crystal in perpendicular direction

Polycrystalline bi-layer BaM film with a negative nucleation field

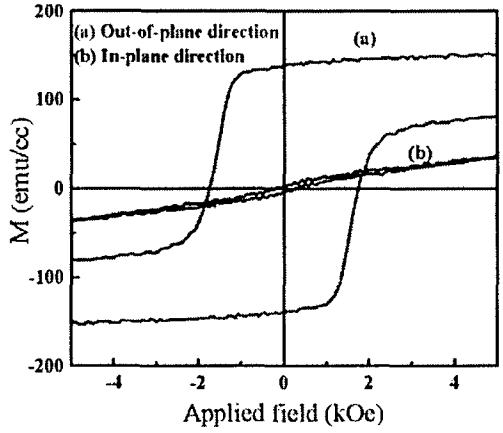

FIG. 8. B-H loops of bi-layer BaM film *ex-situ* heat-treated by complete RTA process

Figure 8 shows the hysteresis loops of a bi-layer BaM film, *ex-situ* annealed by a series of sequential rapid thermal annealing (RTA) process. The heat-treated bi-layer BaM film shows a $4\pi M_S$ of about 2 kG, coercivity (H_c) of 17.5 kOe, and squareness of 0.95 in the out-of-plane direction. Furthermore, the *ex-situ* heat-treated bi-layer film has a large negative nucleation field (H_N) of 1.6 kOe and a significantly higher squareness of 0.95 compared to the squareness of the as-deposited bi-layer film which was 0.41. The negative nucleation field is a negative magnetic field, which is required to start magnetization reversal after saturation of *c*-axis oriented BaM film in the positive field direction. The negative nucleation field of ferrite materials in circulators is an important property for self-biasing. Additionally, the hysteresis loop shows the characteristic perpendicular magnetic anisotropy. Magnetic properties of both as-deposited BaM and *ex-situ* heat-treated BaM are summarized in Table IV.

Table IV. Magnetic properties of bi-layer BaM film at sequent steps of heat treatment

		As-deposited	→ 900 °C (1 min)	→ 1000 °C (5 min)	→ 1100 °C (3 min)
⊥	$4\pi M_s$ (Gauss)	2089	4775	4684	1965
	Coercivity (Oe)	1169	2382	2699	1750
	Squareness	0.41	0.63	0.70	0.95
	Nucleation field (Oe)		730	665	-1600
//	$4\pi M_s$ (Gauss)	1908	4381	3736	792
	Coercivity (Oe)	68	1957	2668	225
	Squareness	0.05	0.27	0.31	0.07

The *ex-situ* heat-treated bi-layer BaM film clearly shows sharp x-ray (000*l*) peaks indicating well crystallized film and secondary phase peaks related to α-Fe_2O_3 (hematite), as shown in Fig. 9. This suggests that the amorphous top layer was crystallized in two different phases of α-Fe_2O_3 and BaM. It has been reported that an intermediate α-Fe_2O_3 phase occurs during the crystallization of amorphous BaM films rather than a direct phase transformation from the amorphous to

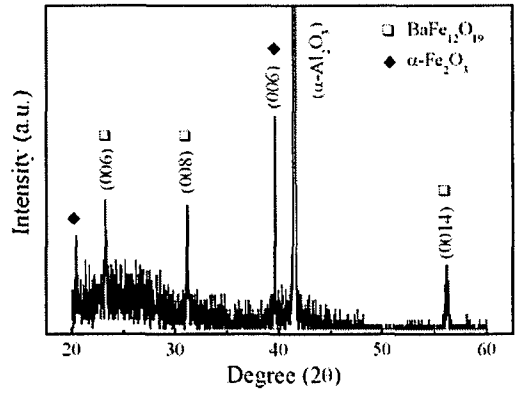

FIG. 9. X-ray diffraction pattern of bi-layer BaM film *ex-situ* heat-treated by complete RTA process

crystalline state. In fact, a phase of α-Fe_2O_3 is observed in the RTA processed BaM film, not phase transforming to crystallize in BaM phase. As a result, the α-Fe_2O_3 phase enhances the *c*-axis orientation in the out-of-plane direction of BaM crystallite from the crystallographic relationship $(000l)_{BaM}$ // $(000l)_{\alpha\text{-}Fe2O3}$ between α-Fe_2O_3 and BaM. This leads to overcoming of the demagnetization field in the *ex-situ* heat-treated bi-layer BaM film

In order to relate surface morphology to magnetic properties, both as-deposited and *ex-situ* heat-treated bi-layer BaM films were characterized by an AFM. The as-deposited film has 10 ~ 20 nm sized nano-crystallites and the roughness is 4.1 nm (root mean square: rms) as shown in Fig. 10 (a). A fine scale roughness (28.1 nm rms) develops after *ex-situ* heat treatment, as shown in Fig. 10 (b). Needle- and plate-like BaM grains with the size of 0.5 ~ 2 μm are observed in the *ex-situ* heat-treated bi-layer BaM films. The easy axis of the needle-like BaM grain is parallel to the short axis dimension, due to the large crystalline anisotropy. This contributes to the enhancement of the *c*-axis orientation

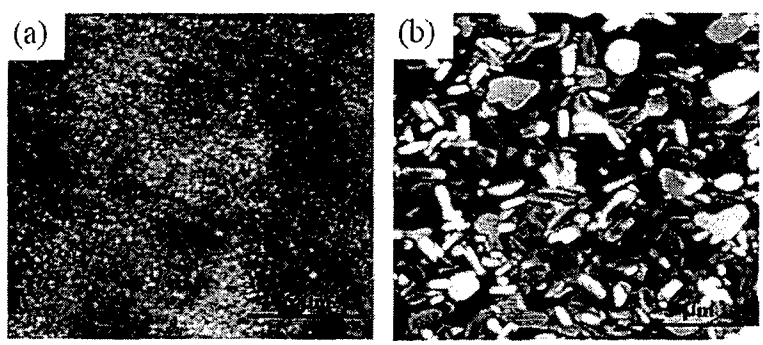

FIG. 10. Surface morphology of (a) as-deposited bi-layer BaM film (b) bi-layer BaM film *ex-situ* heat-treated by complete RTA process

of the BaM film. It is speculative that the nano-crystallites in the as-deposited film act as the nucleation sites for α-Fe_2O_3 and BaM crystallites during the RTA process.

$Ba_3Co_{0.8}Zn_{12}Fe_{24}O_{41}$ hexa-ferrite particles for LTCC substrates

As-shake-milled mixture of $BaCO_3$, CoO, ZnO, and α-Fe_2O_3, was heat-treated at 1350 °C-6hr in air. However, as-heat-treated $Ba_3Co_{0.8}Zn_{1.2}Fe_{24}O_{41}$ hexa-ferrite ($Co_{0.8}Zn_{1.2}Z$) particles has W-type ($Ba_2Me_2Fe_{12}O_{22}$) and non-stoichiometric ferrite. In order to remove secondary phases from the as-heat-treated $Co_{0.8}Zn_{1.2}Z$ particles, the powder was subjected to re-shake milling process to homogenize and nano-sized particles. The re-shake

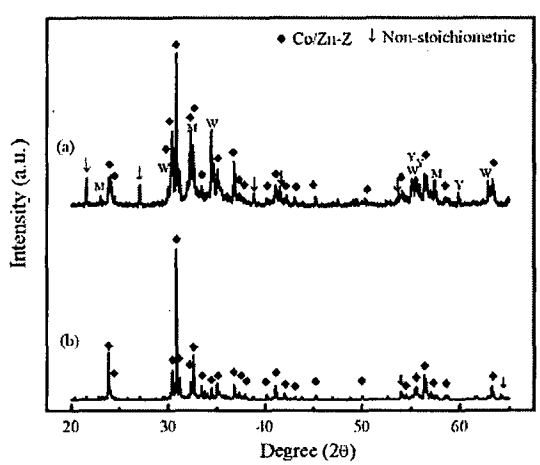

FIG. 11. X-ray patterns of re-heat-treated $Co_{0.8}Zn_{1.2}Z$ powders at 1350 °C-6 h (a) in air and (b) in O_2. [note: M ($BaFe_{12}O_{19}$), Y ($Ba_2Me_2Fe_{12}O_{22}$), W ($BaMe_2Fe_{16}O_{27}$)]

milled $Co_{0.8}Zn_{1.2}Z$ particles were re-heat-treated at 1350 °C for 6 h either in air or in oxygen. As results, small quantities of secondary ferrite phases such as M ($BaFe_{12}O_{19}$), Y ($Ba_2Me_2Fe_{12}O_{22}$), W ($BaMe_2Fe_{16}O_{27}$) ferrites occur in the powder re-heat-treated in air, as shown in Fig. 11(a). On the other hand, as shown in Fig. 11(b), all of the secondary phases disappear from the re-heat treated powder at 1350 °C for 6 h in the oxygen environment. The oxygen environment for the heat treatment remarkably enhances the crystallization of the $Co_{0.8}Zn_{1.2}Z$ single phase. During the high temperature heat-treating process, the oxygen environment prevented the $Co_{0.8}Zn_{1.2}Z$ particles from an oxygen deficiency, resulting in $Co_{0.8}Zn_{1.2}Z$ single phase. The saturation magnetization and coercivity of the re-heat-treated particles in the oxygen environment were found to be 50 emu/g and 9 Oe, respectively.

In order to gain the feasibility of LTCC processing of the studied powders, green disks were made from a mixture of the sintering agent 5 wt% Bi_2O_3 and the re-heat-treated $Co_{0.8}Zn_{1.2}Z$ powder, which was re-heat-treated either in the oxygen environment or in air. The green disks were then sintered at 900 °C for 6 h in air. Both M-type ($BaFe_{12}O_{19}$) and Y-type ($Ba_2Me_2Fe_{12}O_{22}$; Me = Co, Zn) hexa-ferrite phases were identified by x-ray diffraction pattern for low temperature sintered disk, which made from the re-heat-treated $Co_{0.8}Zn_{1.2}Z$ powders in air.
The high coercivity of 606 Oe resulted, as shown in Fig. 12 (a). On the other hand, low temperature sintered disk, made from the re-heat-treated $Co_{0.8}Zn_{1.2}Z$ powder in the oxygen environment, show the major peaks of $Co_{0.8}Zn_{1.2}Z$ phase with minor peaks of M-type hexa-ferrite phase. The trace of secondary M-type phase contributes to the increase of coercivity from 9 Oe of the powder to 20 Oe of low temperature sintered disk as shown in Fig. 12 (b), while maintaining 50 emu/g (at H_{appl} = 10 kOe). It is noted that soft properties of Co_2Z ferrite is subject to the existence of secondary phases. Figure 13 shows frequency dependence of complex permeability and permittivity for low temperature sintered $Co_{0.8}Zn_{1.2}Z$ disk. It is observed that the Cut-off frequency of $Co_{0.8}Zn_{1.2}Z$ sintered disk is around 2.0 GHz, as shown in Fig. 13.

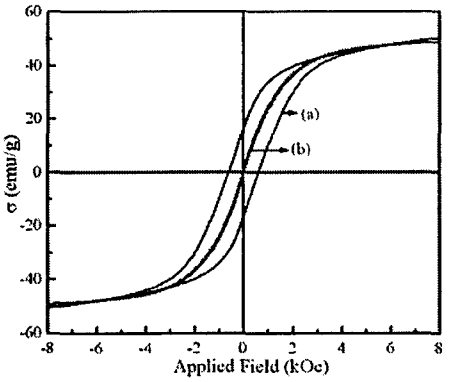

FIG. 12. Hysteresis loops of sintered $Co_{0.8}Zn_{1.2}Z$ disks with 5 wt% Bi_2O_3 sintering agent at 900 °C-6 h in air (a) made from the re-heat-treated powder at 1350 °C in air and (b) made from the re-heat-treated powder at 1350 °C in O_2.

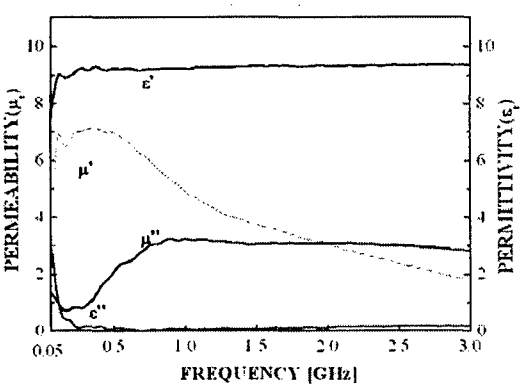

FIG. 13. Frequency dependence of permeability and permittivity for $Co_{0.8}Zn_{1.2}Z$ disks with 5 wt% Bi_2O_3 sintering agent at 900 °C-6 h in air

V. Conclusions

Single crystalline BaM thick film (greater than 100 μm) and BaM single crystals were successfully grown by the LPE process and by a high temperature/slow furnace cooling process. Saturation magnetization, anisotropy field, and coercivity are close to bulk values. The crystallographic BaM thick film was confirmed by analysis of single crystal x-ray diffractometer. Anisotropy field and saturation magnetization of BaM single crystals can be controlled by cation dopants. Polycrystalline BaM thin film possesses a negative nucleation field (-1.6 kOe) and a squareness of (0.95). We now have the capability to grow other ferrite single crystalline films and bulk crystals to meet GHz range device applications. The UI has capabilities to grow single crystalline ferrite thick films and bulk for use in microwave devices.

VI. Future Work

Future work includes:

- Growing of hexaferrite (BaM) thick films.
- Development of composite BaM (> 100 μm) films having a negative nucleation field, high remanent and high coercivity.
- Characterization of microwave properties of BaM thick films and bulk BaM crystals.
- Study grain control mechanism of BaM or other ferrite polycrystalline film having high remanent magnetization.
- Investigation of magnetic domain structure which is dependent on anisotropy field.
- Supplying hexaferrite substrates (large squareness) to the design group (Young's) for GHz range circulator fabrication.

Appendix B

Film Fabrication using Liquid Epitaxy Reflow Method

David N. McIlroy and Wei Jiang Yeh

I. Abstract

Many methods have been tried to grow c-axis oriented magnetoplumbite (BaM) films, such as sputtering [1], pulse laser deposition (PLD) [2], chemical vapor deposition [3] and liquid phase epitaxy (LPE) [4], [5]. Although sputtering and PLD can produce excellent c-axis oriented thin BaM films with low microwave losses [6], the maximum thickness of the films fabricated by the vacuum techniques is around 30 micrometers. Oliver *et al.* [7] have used PLD to grow 28 μm BaM thick films that do not crack or delaminate. Yuan *et al.* [4] have shown that even with slow sputtering deposition rates, films thicker than 3 μm tend to peel from the substrate during annealing. From our own experience, when the film thickness deposited by sputtering is in excess of a few micrometers, the orientation becomes random. It is found that the LPE method is the most effective way to grow thick BaM films with c-axis orientation [4], [5]. Typically, PLD or plasma sputtering is used to grow a seed layer followed by LPE [8]. These thick films have excellent c-axis orientation and a coercivity of approximately 10 Oe, which indicates that they have near single crystal structure. Unfortunately, single crystal BaM films cannot be self-biased due to their low coercivity. Polycrystalline c-axis orientated barium ferrite thick films with moderate coercivity values appear to be the possible solution to the self-biased problem.

During Phase II, we considered two different directions of research. The first one focused on improvements of sputtered BaM thin films, which are used as a seed layer for growing thick films. The second thrust focused on the growth of thick films and bulk BaM.

With respect to the thin film investigation, we successfully grew c-axis oriented BaM thin films (about 0.3 μm thick) on sapphire (0001) substrates by the alternating temperature, multilayered method. Perpendicular-plane and parallel-plane coercivites of about 2.2 kOe 0.07 Oe were obtained; the perpendicular squareness was about 0.88. The same was attempted on MgO(111) substrates with modest success in maintaining c-axis orientation. For the thick film fabrication, we have developed the modified liquid epitaxy reflow (MLPE) method to grow up to 0.5 mm BaM thick films. With this method, a seed BaM layer was not required, which greatly simplified the fabrication process.

In the future, we will use the alternating temperature multilayered method to grow good c-axis oriented BaM thin films on sapphire substrates as a seed layer. We will then use the modified LPE system to grow BaM thick films.

II. Proposal Objectives

The following objectives were listed in the proposal for our group:

Magneton Sputtering: Multilayer techniques in conjunction with magneton sputtering will be employed to grow thick films up to 20-50 μm. If the films show a deficit in barium percentage against iron, barium-enriched targets will be made to adjust the barium to iron ratio. *In-situ* annealing will be used to crystallize the layers after the deposition of each layer. This process will be repeated until the final thickness is achieved. External annealing will also be considered in lieu of the *in-situ* annealing process.

Etching: The etching of the oxide film is a new activity planned for FY05. This activity is necessary as part of the hexaferrite circulator fabrication process. The standard reactive dry etching process, which is fast and suitable for thick films, may not work for oxides. An ion milling process is more suitable for oxides, yet slow, especially for thick films. The third alternative is the wet etch process. All three etching processes along with the deposition of the copper film onto the ferrite will be explored as part of the FY05 effort.

As mentioned below, most of our efforts were focused on sputtering and liquid phase epitaxy techniques. Other than at an exploratory level, the etching task did not receive mush attention.

III. Methodology

During FY06 we developed the alternating temperature multilayered technique to grow c-axis oriented BaM thin films on sapphire (0001) by sputtering. BaM thin films were deposited on a clean 10mm×10mm sapphire (0001) substrate using an RF magnetron sputtering system. A turbo molecular pump was used to reach 3×10^{-6} Torr. The gas pressure during deposition was fixed to about 8×10^{-3} Torr using 20% pure oxygen and 80% pure argon. The target was a commercial barium ferrite 2.0 inch diameter disk placed 2.25 inches from the substrate. The RF power was fixed at 50W and our deposition rate was about 0.1-0.15 μm/h, according to VB-250 vase elliposemeter thickness measurement. During the deposition, the substrate temperature was kept between 930-950°C. After the first layer was deposited the plasma was stopped and the substrate's temperature was reduced to about 800-820°C. The plasma was then resumed to grow another layer at the same condition as the first layer. This procedure was repeated until the final thickness was reached. The thickness of the films was between 0.3-0.5μm. After deposition, the color of the as-grown films was dark brown. The as-grown films show magnetic properties, so no post annealing was required to crystallize the films. That is, the films were grown *in-situ*.

To grow BaM thick films, we developed the modified liquid phase epitaxy reflow method (MLPE). A vacuum LPE system is shown in Figure 1. The MLPE process is a two-step process. First, a barium and iron oxide based powder mixture was ground and thoroughly mixed from powders of barium carbonate ($BaCO_3$), iron oxide (Fe_2O_3) and boron oxide (B_2O_3) in ratios 40:9:10, respectively. A 120 ml quartz crucible heated by a tungsten-coiled heater was placed in a vacuum chamber that was pumped to a base pressure of 30 mTorr. The starting amount of powder mixture occupied half of the volume of the

crucible. The temperature of the crucible was gradually increased to 1300^0C, at which point melt was achieved. To ensure homogeneity, the melt was stirred as long as 12 hours inside the vacuum chamber using a platinum stirrer. The stirrer speed was set to 30 rpm. The operating pressure in the chamber remained below 0.3 Torr. Once we were satisfied with the uniformity of the melt, it was then slowly cooled to room temperature under vacuum. At this point, the solidified substance was amorphous, i.e., without crystal orientation. The second step for obtaining a c-axis oriented BaM thick film was to cut out a small piece from the solidified substance. The approximate weights of these pieces were in the range of 0.03 to 0.05 grams. A piece of the alpha phase BaM was placed onto a polished sapphire (Al_2O_3 with (0001) orientation) substrate. This was then placed in a furnace and heated to 1200^0C in air for one hour to remelt the BaM. The actual formation of the crystals was observed after a slow cool was initiated. The crystallization in the preferred c-axis orientation of the barium ferrite was observed to produce best results at cooling rates between 3 to 5 degrees Celsius per minute. As a result, a thick BaM film was formed on the substrate. The thickness of the film was dependent upon the size of the precut solidified specimen and the size of the substrate. Films with thicknesses of 0.2 to 0.5 mm were routinely obtained.

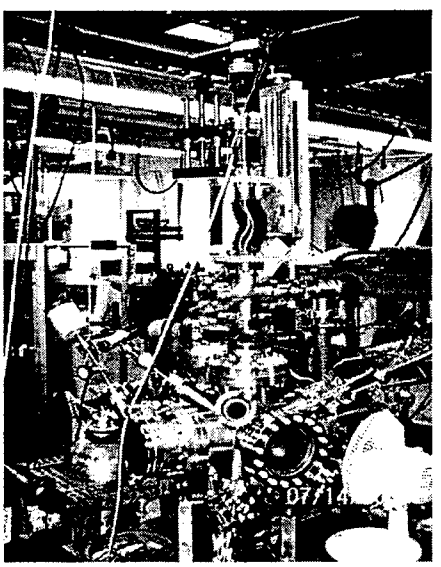

Figure 1: The vacuum LPE

IV. Results and Discussion

BaM Thin Film Results

To study the magnetic properties of our BaM thin films, the magnetization M was measured as a function of the static externally applied field H using a vibrating sample

magnetometer (VSM) at room temperature. In Figure 2, we show the hysteresis loops for both perpendicular and parallel directions of the applied field of a 0.35 μm thin film.

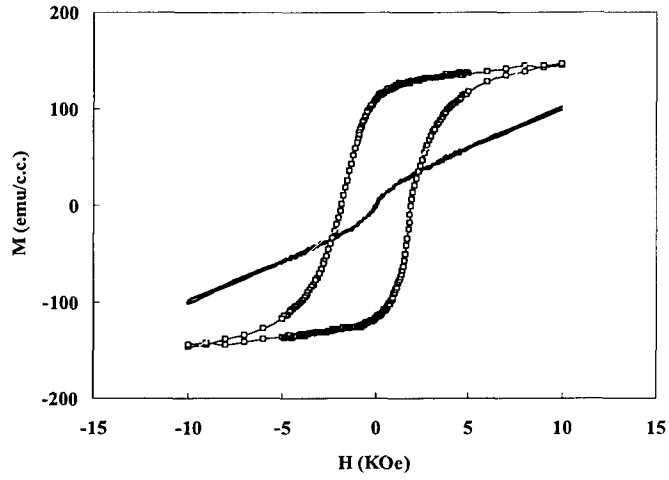

Figure 2: VSM hysteresis loops for a 0.35 μm BaM thin film on (0001) sapphire substrate. The square symbols correspond to an out-of-plane VSM measurement and the solid line to an in-plane VSM measurement.

The measured perpendicular coercivity was about 1.82 kOe and the parallel coercivity was 0.07 kOe. The perpendicular remanent magnetization was about 40 times as large as in-plane ones, which means that the direction of easy magnetization is almost perpendicular to the film plane. The perpendicular squareness S ($S=M_r/M_s$) was moderate and about 0.77. The average saturation magnetization $4\pi M_s$ value was small and of value 1.8 5kG.

The c-axis orientation was verified by the x-ray diffraction data, as shown in Figure 3. In that data, strong 006, 008 and 0014 peaks were observed. The 109 in-plane peak was also observed. These data show that the film was dominated by c-axis orientation.

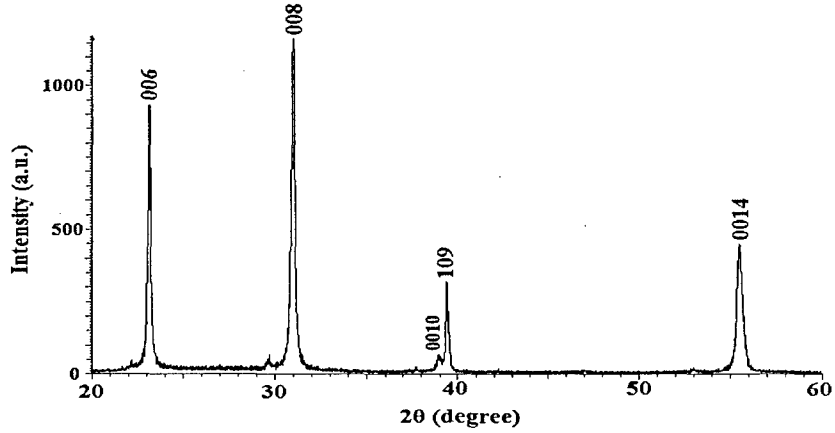

Figure 3: X-ray diffraction diagram of the 0.35μm BaM/ Sapphire film.

Because the lattice constant mismatch is minimal with BaM thin film and MgO(111) (i.e., about 1%), we continued growing BaM thin films on MgO(111). As a result, c-axis orientation was improved significantly. External annealing was used to crystallize the films. A coercivity of about 1,470 Oe was obtained in the perpendicular direction, which was larger than the coercivity in the parallel direction by more than ten times. The saturation magnetization value was in the range of 2,300 G. Figure 4 data shows the measured hysteresis loop for both perpendicular and parallel directions of the 0.15 μm films on MgO (111).

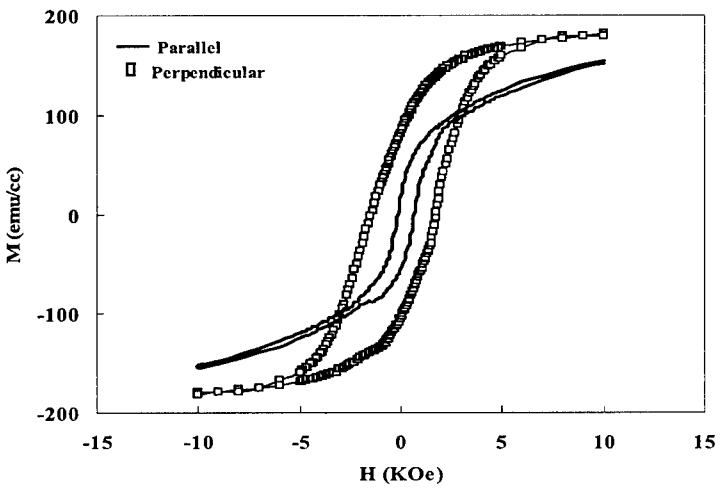

Figure 4: The VSM hysteresis loops for the 0.15μm BaM thin film on MgO (111).

In Figure 5 the x-ray diffraction data of the 0.15 μm films on MgO (111) show good c-axis orientation. The highest intensities of the in-plane peaks (107 and 114) were quenched. Unfortunately, the data exhibits 108 and 218 in-plane peaks and an unidentified peak at 28°. All c-axis orientation major peaks were observed.

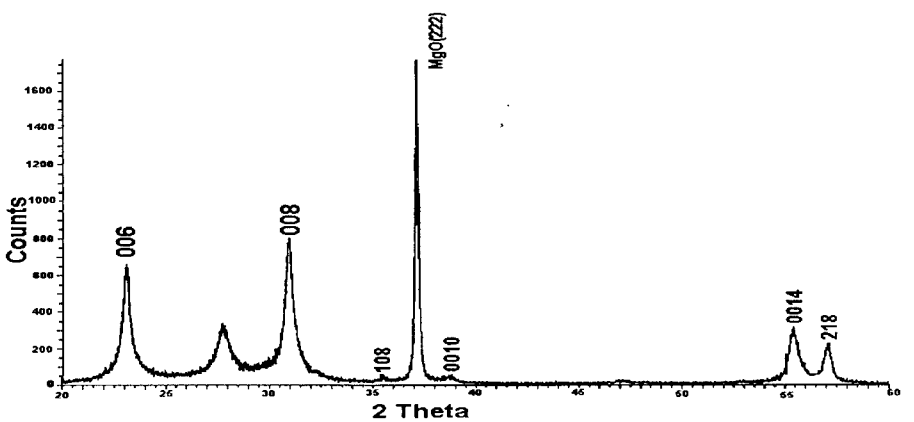

Figure 5: X-ray diffraction diagram for the 0.15μm thin film on MgO (111).

BaM Thick Film Results

We used a vibrating sample magnetometer (VSM) to study the magnetic properties of our thick films. In Figure 6, hysteresis loops for both perpendicular and parallel directions of the applied field of a 350 μm thick film are shown. It can be seen from Figure 6 that both M-H loops are asymmetric. Perpendicular coercivities of about 100 Oe were obtained; the average saturation magnetization was about 2,000 G. We speculate that the fairly large BaM crystals (average width of 20 μm) attribute to the relatively low coercivity value. A possible way to improve the coercivity in the future could be by controlling the cooling rate to facilitate the growth of smaller size crystals.

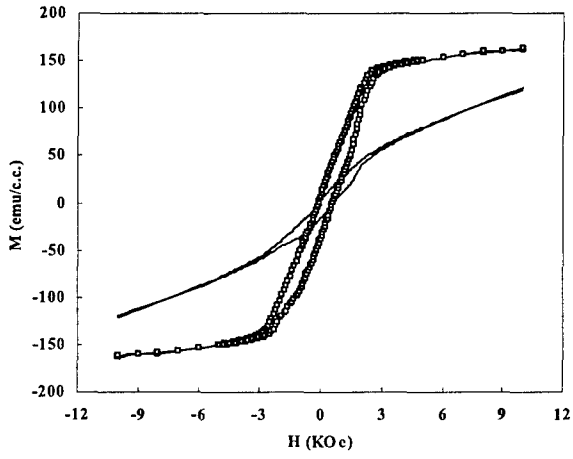

Figure 6: VSM hesteresis loops for the 350 μm BaM thick film on (0001) sapphire Al_2O_3 substrate. The square data symbols correspond to an out-of-plane VSM measurement and the solid line to an in-plane VSM measurement.

To verify the crystal orientation, an X-ray diffraction (XRD) spectrum was measured. The XRD pattern illustrated in Figure 7 shows that the 350 μm thick film has out-of-plane uniaxial anisotropy. It is also observed that the c-axis of the film is aligned normal to the film plane. Intense peaks are identified as the 006, 008 and 0014 reflections of the magnetoplumbite phase.

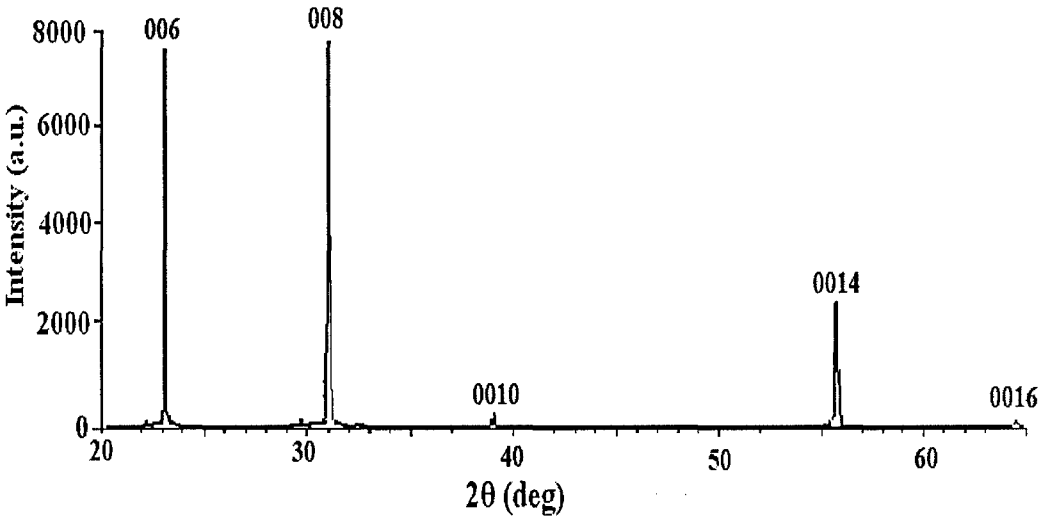

Figure 7: XRD pattern of the 350 μm BaM thick film on (0001) sapphire Al_2O_3 substrate.

Figure 8 shows a SEM image of a typical 350 μm thick BaM film grown on a sapphire (0001) substrate. Here BaM hexagonal platelets can be clearly seen on the surface of the film. They are randomly oriented with respect to each other, but they are all c-axis oriented parallel to the surface normal (out of the plane of the figure). A thickness of 350 μm was measured by cross sectional SEM and is shown in Figure 9.

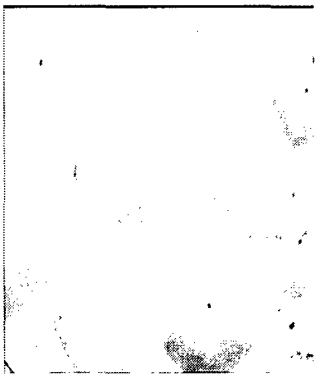

Figure 8: SEM surface image of the 350 μm BaM thick film on sapphire substrate.

Figure 9: SEM cross section image.

V. Future Work

Our goal is to grow self-biased BaM thick film by any means necessary. Our earlier attempts using magnetron sputtering do not appear to have any promise for thick film growth. However, we will attempt to grow good c-axis oriented thin films on either

sapphire (0001) or MgO (111) and use it as seed layer in the LPE system. The main effort in the future will be to grow BaM thick films of c-axis orientation with moderate values of coercivity (about 1,000 Oe) by MLPE. Two methods will be used. One method is to vary the cooling rate to reduce the crystal size, which should increase the coercivity value. The second method is to add some impurity elements to the melt. It is believed that the BaM will crystallize in c-axis and the impurity phase may be pushed out to surrounding places that will form pinning centers that should also increase the coercivity value.

References

1. T. Fujiwara, IEEE Trans. Magn. **21**, 1480 (1985).
2. T. L. Hylton, M. A. Parker, M. Ullah, K. R. Coffey, R. Umphress, and J. K. Howard, J. Appl. Phys. **75**, 5960 (1994).
3. M. Matsuoka, and M. Naoe, J. Appl. Phys. **57**, 4040 (1985).
4. T. S. Cho, S. J. Doh, J. H. Je, J. Appl. Phys. **86**, 1958 (1999).
5. Y. Hoshi and Y. Kubota, IEEE Trans. Magn. **31**, 2782 (1995).
6. Z. Zhuang, M. Rao, D. E. Laughlin, and M. H. Kryder, J. Appl. Phys. **85**, 6142 (1999).
7. X. Sui, and M. H. Kryder, Appl. Phys. Lett. **63**, 1582 (1993).
8. T. L. Hylton, M. A. Parker, and J. K. Howard, Appl. Phys. Lett. **61**, 867 (1992).

Appendix C
FMR Linewidth Measurements

Carl E. Patton and Nan Mo
Colorado State University

I. Abstract

Ferromagnetic resonance (FMR) measurements provide critically important information about microwave loss and relaxation, damping processes, and precessional dynamics in magnetic materials. An FMR spectrometer system based on shorted waveguide technique has been constructed to perform FMR measurements by means of measuring the profiles of absorbed power for absolute power approach and its field derivative for lock-in detection approach versus static magnetic field. The operating frequency can be any frequency, but the designed system was tailored for X-band operation. Tests have been made on polycrystalline yttrium iron garnet materials with a known linewidth. The measurement results using both approaches are in good agreement with previous measurements. Future applications of this system can be made to perform frequency dependent FMR measurements on magnetic bulks and thin films. Further modifications will improve the measurement capabilities, especially angle dependence and wider frequency range.

II. Proposed Objectives:

The recent increasing need for low loss and high frequency magnetic devices, such as isolators, phase shifters, circulators, filters, delay lines, magnetic recording devices has provided an impetus to renew the fundamental understanding of microwave loss and relaxation, damping processes, and precessional dynamics in magnetic materials. Ferromagnetic resonance (FMR) and the FMR linewidth have long been the mainstay for such studies. The objective of this sub-project led by University of Idaho and Colorado State University is to construct FMR spectrometer systems based on a shorted waveguide technique. Currently, the operating frequency is in the range of X-band, roughly 7 - 12 GHz. Two approaches, namely absolute power (AP) and lock-in detection (LID), are used for a given drive frequency. For the AP approach, one measures the profile of microwave power absorbed by a concerning magnetic sample versus external static magnetic field, and extract the FMR field and linewidth through a standard Lorentzian fit of this profile. For the LID approach, a small low frequency sinusoid modulation field (signal A) is further applied to the measuring sample. A lock-in detection method is used to detect the AC signal (signal B) in the absorbed power with the same frequency as signal A. The ratio of signal B to signal A gives the field derivative of the absorbed power and FMR linewidth through a fit to the derivative of Lorentzian curve.

III. Methodology

Measurement System

Figure 1 shows the block diagram of the prototype FMR spectrometer system constructed at Colorado State University. The microwave drive signal is generated by an HP8350B sweeper that can be replaced by other sources, such as a klystron or a Gunn diode. The waveguide system involves two coax-to-waveguide adaptors, a directional coupler, a waveguide short, two isolators, one standard un-calibrated diode detector, and one calibrated detector for the network analyzer. The magnetic sample is mounted on the bottom of the waveguide short on a small nonmagnetic and low microwave loss pedestal or holder. The reflected power is detected by a HP11664E detector connected to a scalar network analyzer and/or a diode detector connected to low noise AC amplifier and a lock-in amplifier. The reference AC signal from the lock-in amplifier drives a set of modulation coils that generate a small AC magnetic field inside the magnet gap. The static field is measured with a gaussmeter and a Hall probe. The sweeper, the network analyzer, the lock-in amplifier, the gaussmeter, and the magnet power supply are connected to a computer though a GPIB card and IEEE-488 interface. A Labview program is installed to perform automatic FMR measurements. This system allows one to measure the power reflection and its derivative as a function of static external field.

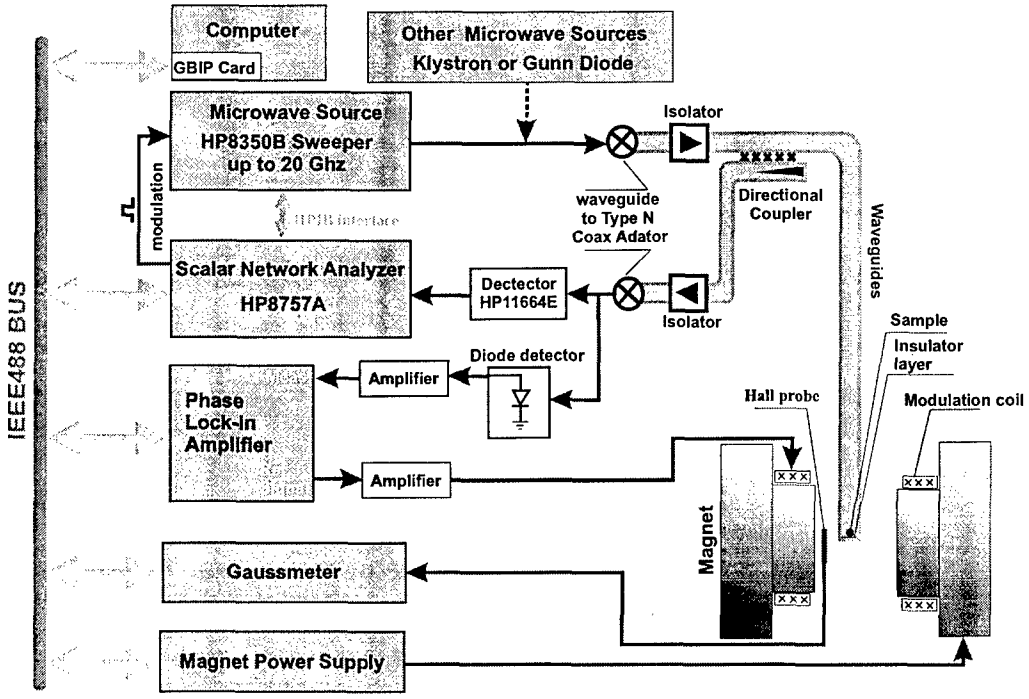

Figure 1: Block diagram of ferromagnetic resonance spectrometer using shorted waveguide.

Absolute Power Approach

The modulation coils and lock-in amplifier are not used for this configuration. The power reflection is detected by HP11664 detector and network analyzer. The power reflection coefficient is measured as a function of the static external field. This curve has a background response that is typically field independent. The background level can be found by applying a field far from resonance. The observed power absorption signal is this background level minus the loss dip associated with the FMR absorption. A standard Lorentzian fit of the loss dip gives the FMR field and the field linewidth at half maximum.

Lock-in Detection Approach

The network analyzer is not used for this case. The modulation coils are driven by a reference AC signal generated by the lock-in amplifier. This drives the modulation coils and adds an AC component to the field in the magnet gap. Typically, a frequency in the 300 Hz range is used and the modulation field is kept to a small amplitude, well below the linewidth of the FMR response. The in-phase AC component of the reflected signal from the short at the reference or modulation frequency is the signal of interest. The lock-in amplifier detects this signal amplitude. This amplitude is proportional to the derivative of the actual FMR power absorption dip, provided that the modulation amplitude is small. One measures this signal as a function of the static bias field. A derivative Lorentzian fit of this field function gives the FMR field and the full width at half maximum (FWHM) FMR linewidth in field units. An alternative way is to directly evaluate the field width from the field separations of the two oppositely signed peaks in the derivative response, a peak to a dip near resonance, which is called the derivative (DER) linewidth. For a Lorentzian FMR absorption power dip, the FWHM linewidth is equal to $\sqrt{3}$ times the PP linewidth.

IV. Results

The representative measurements shown below were made on a near theoretical density polycrystalline yttrium iron garnet samples produced by hot isostatic pressing, taken as a calibration sample. The magnetic properties of this sample are well established. See *A. V. Nazarov, D. Ménard, J. J. Green, C. E. Patton, G. M. Argentina, and H. J. Van Hook, J. Appl. Phys. 94, 7228 (2003).* The nominal FWHM linewidth of this sample is 13 Oe at 9.5 GHz. The measurements shown below were made on a nominal 2 mm diameter polished spheres at a nominal frequency of 9.5 GHz.

Absolute Power Approach

Figure 2 shows the measurement results based on absolute power approach. The sweeper was operated at a center frequency of 9.5 GHz with a very small swept range of 2 MHz. For a given field, the network analyzer reads 201 power points that are uniformly distributed in this frequency range. The average of all these points is then taken to reduce the noise signal. This allows for an accurate measurement of the reflected power $P(H)$

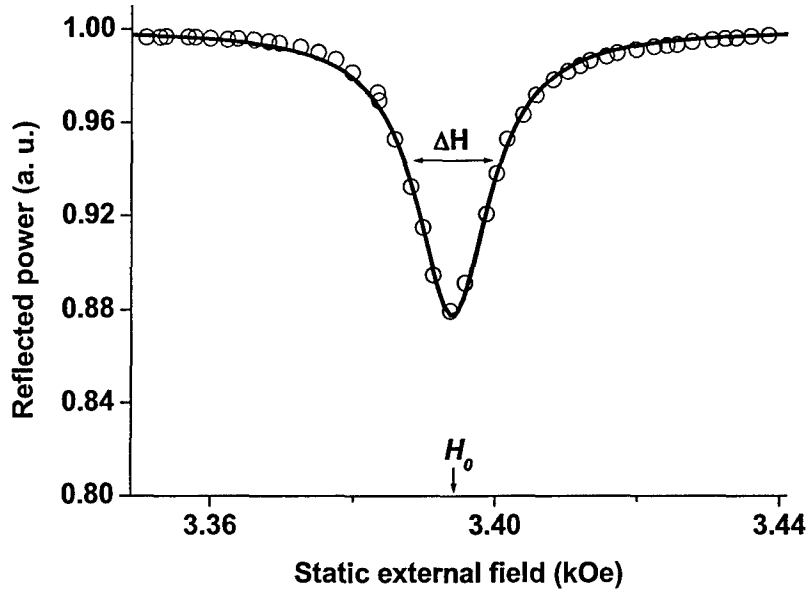

Figure 2: The reflected power as a function of static external field. The open circles show the measurement data while the solid curve shows the Lorentzian fit to these data. The FMR field H_0 and half power linewidth ΔH are also indicated.

as a function of static external field H when the field is swept. The data are shown by the open circles in Fig. 2.

This response of the reflected power versus field is modeled as

$$P(H) = P_{in} - \frac{A}{(H - H_0)^2 + \Delta H^2 / 4},$$

where P_{in} is the input power, A is a constant related to the maximum absorbed power, H_0 is the FMR field, and ΔH is the FWHM linewidth. This is a standard Lorentzian function. The fit to the data, as indicated by the solid curve in Figure 2, gives $H_0 = 3.39$ kOe and $\Delta H = 12.7$ Oe. The above-measured linewidth is in good agreement with the literature value of the linewidth of 13 Oe.

Lock-In Detection Approach

Figure 3 shows measurement results based on the lock-in detection approach. The sweeper operates in CW mode at 9.5 GHz. The lock-in amplifier picks up only the AC component of the reflected power signal at the modulation frequency, 330 Hz in this case. Through signal averaging in the lock-in amplifier by means of an increase in the integration time constant, the noise in this derivative signal can be reduced. If a long

time constant is used, however, care must be taken to sweep the field slowly. The amplitude $|D(H)|$ of this AC signal is field dependent. The amplitude with the phase taken into account gives an output that is proportional to the derivative of absorbed power. The $D(H)$ data are indicated by the open circles in Figure 3. The field separation of the extrema corresponds to the derivative, or peak to peak linewidth, ΔH_{pp}, is obtained as 7.7 Oe. This is indicated in Fig. 3. The middle field between peak and dip is the FMR field. The half power linewidth is obtained to yield $\Delta H = \sqrt{3} \cdot \Delta H_{pp} = 13.3$ Oe .This linewidth is very close to the cited value.

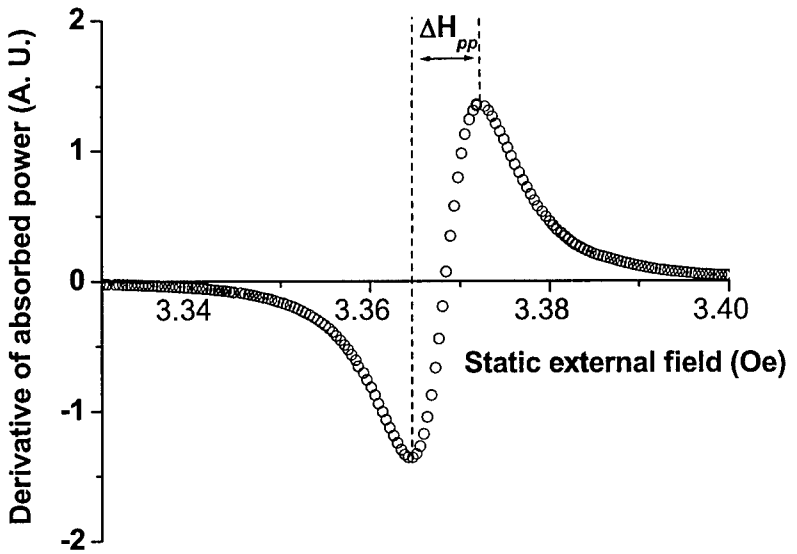

Figure 3: The derivative of absorbed power as a function of static external field. The open circles show the data. The peak-to-peak linewidth ΔH_{pp} is also indicated.

V. FUTURE WORK

Two major enhancements can be made in the future. (a) One can install a rotational base under the magnet. This makes angle-resolved FMR measurements of the FMR field and linewidth possible. The angle dependence is especially important for magnetic thin films. Basic FMR measurements on films can be used to provide noninvasive and intrinsic measurements of the magnetization, various anisotropies that may be present, the gyromagnetic ratio, and the damping. (b) One can modify the microwave source so that measurements can be made in a wide frequency range up to 70 GHz. This could be very important for high anisotropy materials such as barium ferrite in either bulk or thin film form.

Appendix D

Micromagnetic Modeling

Richard Wells

I. Abstract

The micromagnetics group has successfully modeled the M-H characteristics of the polycrystalline films reported by the materials team. Hysteresis loop characteristics for both in-plane and normal fields are accurately reproduced. We have also obtained some preliminary predictions for improved schemes for initially magnetizing these films to help control variations expected to occur due to film M-H squareness that are less than one. We have carried out an analysis of the feasibility of biasing single-crystal thick films produced by LPE methods and have concluded that it does not appear to be practical to bias these films using additional hard magnet films.

Successful modeling of the polycrystalline films required the incorporation of a thermal energy term [1], [6] as reported in the FY04 report. We have also obtained additional experimental evidence and theoretical analyses supporting our magnetic phase hypothesis reported in the FY04 report. The experimental evidence was obtained from analysis of measured torque curve data reported by Dr. Hong's laboratory. We find that to be consistent with both the measured M-H VSM data and measured torque curve results it is necessary to posit the anisotropy energy density equation in a form comprised of a weighted mix of uniaxial and direction cosine terms. This is despite the fact that the films themselves have only HCP crystalline phase. Magnetic phase is not the same as crystalline phase in our terminology although we do bow to tradition and call the two terms in the anisotropy energy expression "HCP" and "FCC" magnetic phases.

Extraction of the relevant parameters for the Polder tensor as well as all other design specification data required by the circulator design team should now be straightforward using the micromagnetic model, either by the direct sinusoid method or by the frequency domain method discussed in the FY04 report.

II. Proposal Objectives

Model micromagnetic phenomenon to estimate the macroscopic magnetic properties of ferrite thick films. Such properties to include saturation magnetization, coercivity, remanence, and effective internal field. Develop method for extracting Polder terms and analyze FMR characteristics.

III. Research Methodology

A 3-dimensional micromagnetic simulator is used to carry out the main calculations to determine material properties. The calculations minimize phenomenological free energy terms [2] constrained by time-domain dynamics of the stochastic Landau-Lifshitz-Gilbert

(LLG) equation. The free energy terms employed include magnetostatic energy, demagnetizing energy, magnetocrystalline anisotropy energy, exchange energy, and thermal energy [6]. Our model was verified against the NIST benchmark models (non-stochastic mode). We use a 3-dimensional grid of unit hexagon calculation cells. Demagnetization is computed using the Zhu matrix method [3] for the structure constants and the Fast Fourier Transform (FFT) for the dynamical field calculations [4].

The first step in modeling a material specimen is to fit its perpendicular and longitudinal hysteresis loop properties through adjustment of the phenomenological energy density parameters. We require that the fits for both loops accurately match vibrating sample magnetometer (VSM) data for the material. In addition we require that postulated anisotropy energy expressions be consistent with the findings of torque curve measurement data obtained on the experimental films. We note that significant errors can occur in the determination of relative anisotropy coefficient ratios if the applied field used for making the torque curve measurement fails to saturate the material for both the longitudinal and the perpendicular loops. In the case of the longitudinal (hard axis) loops this requires a biasing field on the order of about 13kOe to ensure saturation in the hard axis direction.

The size of the calculation volume is determined by analysis of size-dependent shape anisotropy effects on the M-H loop characteristics due to demagnetization. Hysteresis loops for model samples of different sizes are compared and the smallest sample size beyond which no significant additional demagnetizing field effects are in evidence is used for our other calculations.

For hard (polycrystalline) materials we evaluate both the local and the sample-average magnitudes, directions, and time domain dynamics of the magnetization vector and the various effective fields (demagnetizing, anisotropy, and exchange) under simulated conditions of applied bias field and applied ac fields. Complex susceptibility terms in the Polder matrix will be analyzed from magnitude and phase responses of the sample-average magnetization at frequencies of interest to the microwave devices group. This evaluation can be carried out at any desired strength of applied ac field.

Micromagnetic calculations are carried out using both individual high-performance personal computers and on a small workstation cluster. The cluster allows us to run simultaneous parallel simulations. The cluster consists of ten HP PA RISC processors with 1 GB of RAM memory each and 1 TB of disk storage. Each processor has 1 GFLOP/sec arithmetic performance and the cluster as a whole achieves almost 10 GFLOP/sec performance.

IV. Results and Discussion

A. Polycrystalline Hard Materials

We have obtained excellent agreement with the VSM measurements of the polycrystalline BaFe films. Results are also consistent with measured torque curve results although in the case of the longitudinal loops we conclude it is necessary for the

measurement to be performed at a higher level of applied field than is used for the perpendicular characteristics. Figure 1 compares one of our model M-H loops against the experimental data. As shown, both in-plane (longitudinal) and out-of-plane (perpendicular) loops agree very well with the theoretical calculations.

In order to reproduce the experimental loops we found it necessary to incorporate two non-standard energy terms into the micromagnetic dynamics. The first concerns the form of the anisotropy model. It has long been commonly assumed that the anisotropy energy density follows a single phenomenological form, which in the BaFe case is the uniaxial anisotropy equation $E_a = K_1 \sin^2(\theta) + K_2 \sin^4(\theta)$, where θ is the angle between M and the magnetocrystalline easy axis. We found that neither this simple expression nor expansion of this expression to higher power terms could reproduce both loops with the same parameter settings. To reproduce both loops with the same model we found it necessary to make the hypothesis that there also is an anisotropy energy term in the form of the standard direction-cosine expression usually associated with FCC-phase materials. At first we thought this indicated that the real material was being produced with both HCP and FCC phases, but this turned out to not be the case. The actual material is pure HCP-phase. After this was verified, we began referring to our anisotropy model terms as "magnetic phases" to distinguish the phenomenological energy equation from the crystal structure of the material.

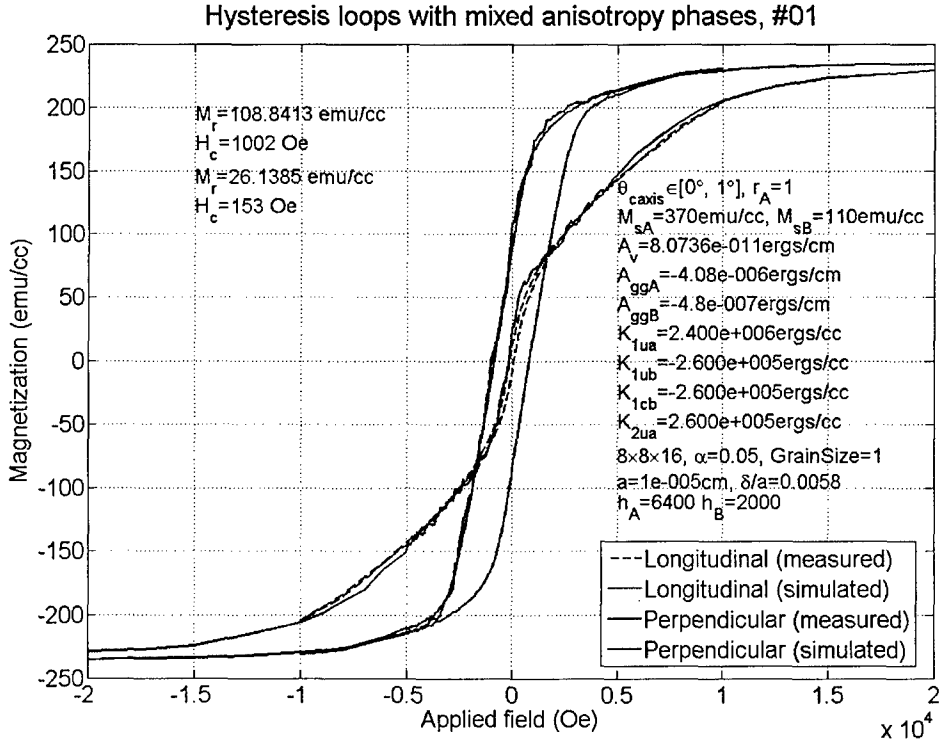

Figure 1: Normal and in-plane M-H loops for one of Hong's polycrystalline films. The blue curve is the loop normal to the film plane. The red curve is the in-plane loop. Black curves are VSM data.

In the absence of magnetic FCC phase anisotropy the coercivity of the longitudinal loop is nearly 0, whereas in the measured M-H loops this coercivity is on the order of about 100 Oe. In addition, the longitudinal loop exhibits an "S" shape (figure 1), an effect that is not reproduced by models containing only uniaxial anisotropy terms.

We first reported the magnetic phase hypothesis in the FY04 report. Since that time we have carried out additional theoretical evaluations of the implications presented in the classic solid state physics papers dealing with the physical origin of magnetocrystalline anisotropy. It is widely agreed that the principal mechanism of magnetocrystalline anisotropy is spin-orbit coupling and so-called "orbital valence" according to a classical paper by Van Vleck [5]. However, in the case of ferrites there is some contention about this interpretation when the material contains Fe^{3+} ions in the lattice and quenching of the orbital angular momentum results. This is discussed by Wolf [7]. Our hypothesis for a magnetic phase mechanism appears to be compatible with theoretical treatments in which sublattice sites (2a, 2b) are expected to make different contributions to the anisotropy energy [10]-[11]. A number of reports appear to point in the direction of this interpretation of the theory [8-11] although the underlying theoretical picture is by no means regarded as unequivocally established.

The second energy contribution is made by the incorporation of a thermal energy expression [6] as part of the total energy density. With the thermal term incorporated our simulation solves the stochastic LLG (S-LLG) equation using Stratonovich stochastic calculus implemented using Heun's method [6]. One consequence of incorporating this effect is the introduction of a coupling between the thermal energy parameters and the LLG damping coefficient α. We have not been able to confirm whether α might be predictable on the basis of the thermal energy term and so we use experimental FMR data to set the value for α in our simulations.

B. Biasing

Of the material properties we have had to examine to date, the polycrystalline "hard" materials produced by Dr. Hong's lab appear to be the best-suited for the circulator application to date. There are two points in favor of this material: 1. The material is self-biasing; 2. The material has lower coercivity loops in the film plane, which means that the material is "soft" in the x-y plane, promoting higher x-y plane permeability and lower distortion of the ac waveform. The primary issue, of course, is thickness. The films we have seen from Dr. Yeh's lab have a similar attractiveness insofar as the M-H properties normal to the film plane are concerned. The issue that we see with these films is the presence of relatively high H_c in the in-plane direction, which will most likely be a source of non-linear distortion in the ac response. More recent films show some promise that improvement in the in-plane coercivity curve for these films is going to be achieved.

The "cigar-shaped" crystallites produced in Dr. McIlroy's lab are potentially interesting as a means to use shape anisotropy biasing. However, I have had the impression that Dr. McIlroy does not regard these as far-enough-along yet, and we have done no modeling work on them.

As for Dr. Hong's single-crystal thick film, I see no practical means of self-biasing this film other than through the use of shape anisotropy. If it is possible to fabricate a thick non-magnetic binder and etch or otherwise create cylindrical "shafts" in which the film could be grown, then it might be possible to produce shape-biased films. Aside from the fabrication issues this might involve, the key parameters here would be the diameters of the ferrite "flutes" and their packing density. The "flutes" would have to be thin enough to prevent the formation of Bloch walls traversing the z-direction (otherwise the material would be "soft" and non-self-biasing). Neel wall formation at the top and bottom surfaces would probably be okay. We have done no calculations yet that would better define the diameter requirements or the packing density. A rough guess would put the packing density in the range of about 0.6, roughly the packing density of Fe_2O_3 ferrites in old-style "brown" disc and tape recording media.

The aspect ratio of the puck has a direct effect on the amount of demagnetization the material will experience. Defining aspect ratio as puck diameter/puck thickness, in general H_D will increase toward its limiting value of $4\pi M_s$ as the aspect ratio increases. Consequently, the squareness of the normal induction curve can be expected to decrease as aspect ratio increases. Although strictly speaking no "demagnetizing factor" can be defined for a cylindrical puck of aspect ratio r, an approximate demagnetizing factor based on approximating the puck as an oblate spheroid can be used. This factor is given by

$$N_z \approx \frac{4\pi r^2}{r^2-1}\left(1-\sqrt{\frac{1}{r^2-1}}\cdot\sin^{-1}\left[\frac{\sqrt{r^2-1}}{r}\right]\right).$$

The total demagnetization field in the puck is produced by surface magnetic charges on the top and bottom. One way to reduce total demagnetization is to take advantage of the fact that microwave circulator action occurs primarily in the outer annulus of the puck and that the center of the puck contributes very little to circulator action. This suggests that rather than fighting demagnetization through material characteristics we might instead combat the effect by a different scheme of magnetizing the puck. This idea is illustrated in Figure 2 below.

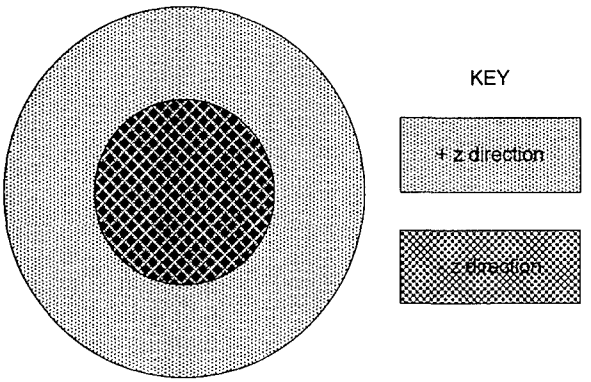

Figure 2: A depiction of the dual-directed puck magnetization scheme. Rather than initially magnetizing the puck uniformly in one direction, we would instead build a special magnetizer so that the center of the puck is magnetized in the – z direction, while the outer annulus of the puck is magnetized in the + z direction. This scheme reduces the total surface magnetic charge on the puck, thereby reducing the intensity of the internal demagnetizing field.

V. Future Work

The micromagnetic simulator work is drawing to a close. The principal remaining activities are documentary. Most of this documentation will be contained in Feng's doctoral dissertation, which is expected to be completed during Summer '06. The dissertation will also include sections discussing the following:

1. Losses in partially saturated ferrites.
2. Polder tensor characteristics in unsaturated ferrites.
3. Internal field characteristics for self-biased high-anisotropy ferrites.
4. Determination of the anisotropy field and accuracy of this determination.
5. Discussion of the feasibility of creating a self-biased, fully-saturated ferrite puck.

Additionally, Dr. Wells will provide to the other members of the group tutorial explanations of the topics of crystal anisotropy, shape anisotropy, domain wall motion and rotation, closure domains, and the load-line concept in designing devices that employ ferrites. These will be provided on an as-requested basis to the team members.

VI. References

1. Victora, R.H., "Predicted time dependence of the switching field for magnetic materials," *Phys. Rev. Lttr*, vol. 63, no. 4, pp. 457-460, 1989.
2. Brown, W.F., Jr., *Micromagnetics*, Malabar, FL, Krieger Publications, 1979.
3. Zhu, J.-G., Interactive Phenomena in Magnetic Thin Films, Ph.D. Dissert., University of California at San Diego, 1989.
4. Xie, F., *A Micromagnetic Model of Hexaferrite and Some Simulation Results*, M.S.

Thesis, the University of Idaho, June, 2004.
5. Van Vleck, J.H., "On the anisotropy of cubic ferromagnetic crystals," *Phys. Rev.*, vol. 52, pp. 1178-1198, 1937.
6. Garcia-Palacios, J.L. and Lazaro, F.J., "Langevin-dynamics study of the dynamical properties of small magnetic particles," *Phys. Rev. B*, vol. 58, no. 22, pp. 14937-14958, 1998.
7. Wolf, W.P., "Effect of crystalline electric fields on ferromagnetic anisotropy," *Phys. Rev.*, vol. 108, no. 5, pp. 1152-1157, 1957.
8. Slonczewski, J.C., "Origin of magnetic anisotropy in $Co_2Fe_{3-x}O_4$," *J. Appl. Phys.*, vol. 29, no. 1, pp. 448-449, 1958.
9. Slonczewski, J.C., "Origin of magnetic anisotropy in cobalt-substituted magnetite," *Phys. Rev.*, vol. 110, no. 6, pp. 1341-1348, 1958.
10. Lotgering, F.K., P.R. Locher, and R.P. van Stapele, "Anisotropy of hexagonal ferrites with M, W and Y structures containing Fe^{3+} and Fe^{2+} as magnetic ions," *Phys. Chem. Solids* **41**, pp. 481-487, 1980.
11. Slonczewski, J.C., "Anisotropy and magnetostriction in magnetic oxides," *J. Appl. Phys.*, vol. 32S, no. 3, pp. 253S-263S, 1961.

Appendix E

Microwave Circuit Design

Jeffrey L. Young

I. Abstract

The principle activities of Microwave Devices Group during Phase II were to 1) fabricate prototype microwave circulator devices for either wideband or high isolation applications, 2) to develop design and analysis tools for the same and 3) to expand experimental capability in microwave components, antennas and ferromagnetic resonance (FMR) testing. The group enjoyed a high level of productivity during this phase by fabricating two additional devices (for a total of five since the inauguration of Phase One) and by solidifying its design, analysis and measurement techniques.

The first circulator constructed during Phase II used a novel, square geometry that allowed for microwave energy to be routed along 90° paths instead of the traditional 120° paths of its circular counterpart. This square circulator achieved about 14 dB of isolation over 2 GHz bandwidth centered at 10 GHz. The second device was designed for broadband performance over the range 6 GHz to 16 GHz. According to simulation studies, the predicted performance was about 20 dB of isolation. Unfortunately, the measured results were less favorable. However, upon closer scrutiny of the device, the Group discovered that the vender that fabricated the device used the wrong ferrite. A new prototype is slated to be constructed during Phase III.

The Microwave Group spent a considerable amount of time developing various measurement techniques and analysis tools for the project. The measurement techniques focused on precision, three-port de-embedding to allow for experimental, rather than numerical, characterization of the circulator. This experimental characterization is necessary for high precision design. Analysis tools were also constructed that quantify the circulator's best case loss scenario. Finally, a new circulator model was devised that is highly accurate and rapid to compute. This model will be used as part of the kernel of an optimization procedure that requires multiple evaluations.

With respect to experimental work, the Group initiated the construction of a new five meter, 2-40 GHz anechoic chamber and a new FMR system. The construction of the chamber began during Phase II and is scheduled to be completed during Phase III. At the close of Phase II, the chamber's carcass was assembled, the positioning equipment was installed and the instrumentation was procured. Phase III activities include the writing of the data acquisition and control software, and the installation of the absorbing, carbon material. The FMR system was designed and configured by Colorado State University (CSU), which functioned as a subcontractor, under the supervision of Prof. Carl Patton. The system was demonstrated to the team to be quite effective.

II. Proposal Objectives:

The primary objective for the Microwave Device Group is to analyze, design, simulate, fabricate and test wideband, microstrip circulators for X- or K-band operation. Specifically, the proposal states that "Novel circulator topologies will be considered that result in wideband, efficient operation while maintaining a compact layout. This will be accomplished by employing the numerous microwave design and analysis tools developed or procured during FY04. Techniques of circulator integration with traditional microwave devices, such as amplifiers and antennas, will be investigated with the goal of eliminating inefficiencies and redundancies in the system. In-plane circulators in conjunction with coplanar waveguide topologies will also be considered. Finally, spin wave simulations and analyses will be conducted in collaboration with Colorado State University."

III. Methodology:

During the course of Phase II, the Microwave Group spent considerable effort devising various equations and models that quantify a circulator's total microwave loss for certain idealized conditions. As is well known, the quality of a circulator's isolation, return loss and insertion loss is dependent on the match between the load impedance and the impedance for perfect circulation. However, when loss is present in the ferrite, it is impossible to achieve perfect isolation, return loss and insertion loss, even if these two impedances are properly matched. With this in mind, the group devised a set of equations that quantify the best case performance when the circulator is designed for perfect isolation or perfect return loss. These loss equations are based upon measured or calculated scattering parameters of the device. If the parameters are measured, then the parameters contain all loss mechanisms associated with Ohmic heating, dielectric losses, radiation, surface waves, spin wave coupling, FMR relaxation, etc. If they are obtained from simulation, then only Ohmic heating, dielectric loss and FMR relaxation are included. Either way, the Group has developed a way of predicting the absolute best case scenario of any device that it intends to fabricate. Devices that exhibit poor characteristics using this methodology are immediately discarded and are not considered for fabrication.

As an example, consider Trans-Tech TT1-2000 bulk magnesium ferrite which has material parameters of $4\pi M_s$=2,000 G, ΔH = 300 Oe, ε_f = 12, $\tan\delta_f$ = 0.00025, and H_c = 1.6 Oe. To minimize loss, the applied field was set at 1,710 Oe, which created an internal field of approximately zero. For purposes of illustration, the ferrite puck is given a radius of 2.5 mm and a height of 0.5 mm. To validate the methodology we chose to obtain the scattering parameters via simulation rather than measurement. (Measurement data will be obtained during Phase III.) Two sets of best case data were calculated; see Figures 1 and 2.

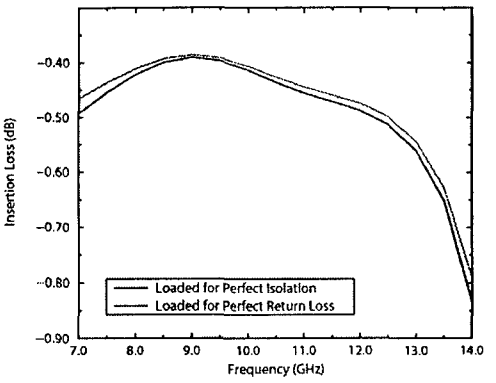

Figure 1

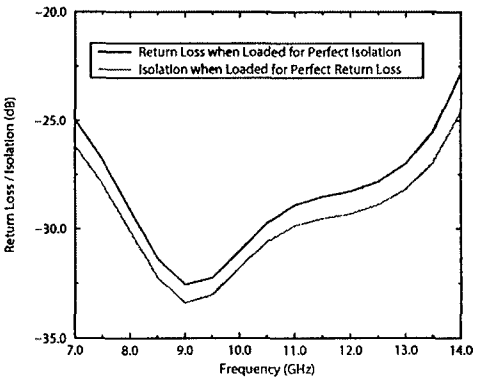

Figure 2

Figure 1 shows the best case insertion loss when the circulator is designed for perfect isolation and for perfect return loss. Figure 2 shows the best case return loss when the circulator is designed for perfect isolation and the best case isolation when the circulator is designed for perfect return loss. Clearly, if the impedances are well match, it will be possible, by definition, to achieve return losses and isolations on the order of 25 to 30 dB over the entire frequency band. Best case insertion losses range from 0.4 dB to about 0.85 dB. If such numbers were unacceptable, then this particular ferrite configuration would be discarded and another configuration would be considered and evaluated.

To expedite the design process and to optimize the device, a new two-dimensional (2D) waveguide model of a three-dimensional (3D) microstrip circulator was devised, as shown in Figure 3. The sidewalls of the waveguide model are perfect magnetic conductors (PMC); the top and bottom walls are perfect electric conductors (PEC). These types of conductors allow for TEM wave propagation with the electric field being normal to the PEC walls and with the magnetic field being normal to the PMC walls. The width of the waveguide is set to be the effective width of the microstrip. This effective width is larger than the actual microstrip width to account for field fringing. Similarly, the region surrounding the puck is also larger to account for field fringing and for wave motion azimuthally about the ferrite puck. The key attribute of this model over its 3D counterpart is one of computational speed. A numerical analysis of the 2D configuration takes minutes; the numerical analysis of the 3D configuration takes hours. As seen in Figure 4, which shows comparative data for the circulation impedance, the results from the 2D model are exceptional.

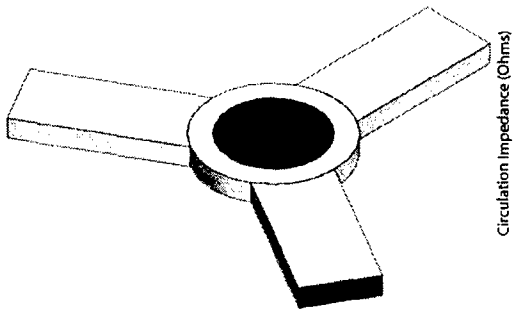

Figure 3

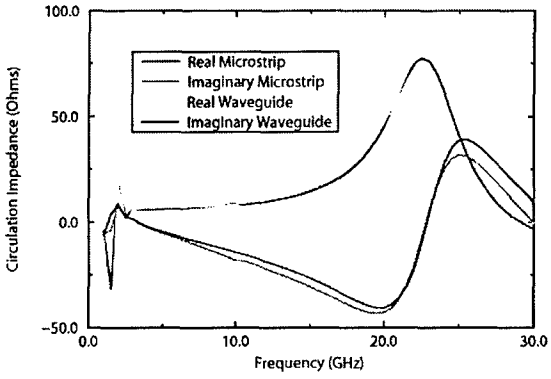

Figure 4

Another activity of Phase II was an investigation into co-planar waveguide circulators. Co-planar ferrite topologies are advantageous from the perspective that the magnetization vector tends to lie in the plane of the ferrite, which is a natural minimum energy condition for certain ferrites. However, from a device point of view, the Group concluded, after conducting numerous simulations and analytical investigations, that the losses for these devices are unacceptable to make co-planar topologies practical. For this reason, this particular activity was terminated.

IV. Results

The first device that was constructed was a novel, microwave circulator employing a square ferrite, as shown in Figure 5. For this device, Trans-Tech TT1-2000 bulk magnesium ferrite was chosen. This ferrite has the following parameters: $4\pi M_s$=2,000 G, ΔH = 300 Oe, ε_f = 12, $\tan\delta_f$ = 0.00025, and H_c = 1.6 Oe. The applied field was chosen to be 1,710 Oe, which created an internal field of approximately zero. The ferrite is 3.1 mm wide and 5.37 mm long, and is embedded in a uniform dielectric made up of D4 Cordierite, which has a dielectric constant of 4.5, a loss tangent 0.0002 and thickness equal to 0.5 mm. The ferrite/dielectric combination is clad with a copper ground plane; copper traces are patterned on top so that each port is centered on its respective edge of the ferrite. The microstrip traces comprising each port have widths of 2.51 mm.

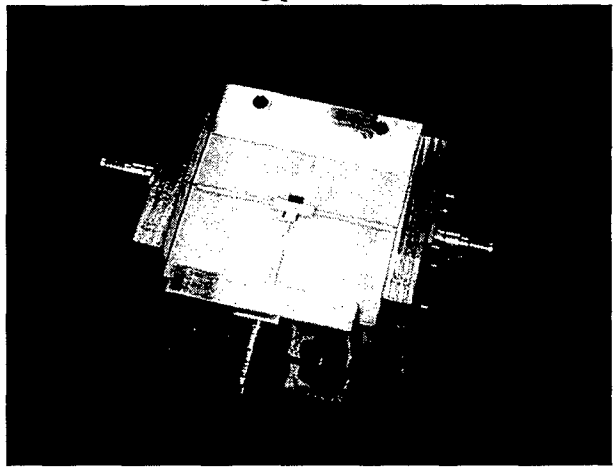

Figure 5

To assure that the correct circulation impedance was realized, a set of matching networks were designed and connected to the ports of the ferrite. One matching network was used for the center port; the other matching network was used for the other two ports. Circulation impedance data for these two networks are shown in Figures 6 and 7. The resonant effect seen in Figure 6 creates a good 50 Ohm match, but over a limited bandwidth. The data of Figure 7 show a broadband characteristic, but with low impedance. As a result, this device is predicted to have a bandwidth of about 20% or so.

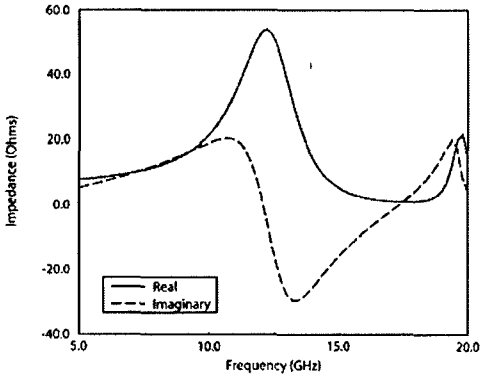

Figure 6

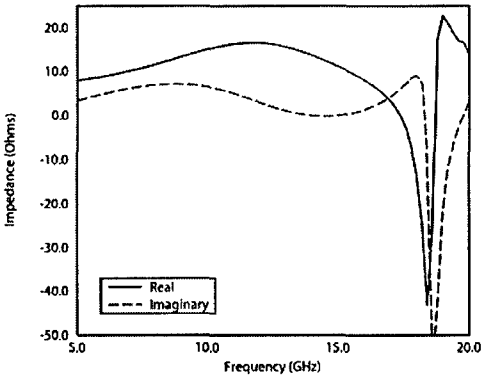

Figure 7

Consider the measured S-parameter data, which are shown in Figures 8, 9 and 10. The data includes test fixture connector effects.

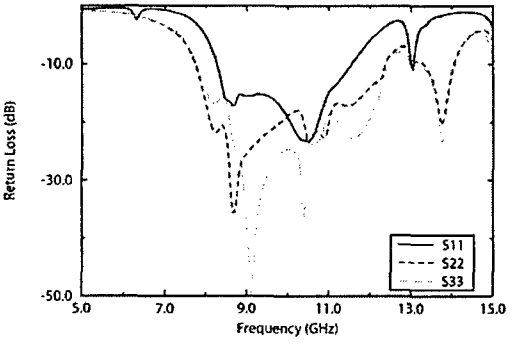

Figure 8

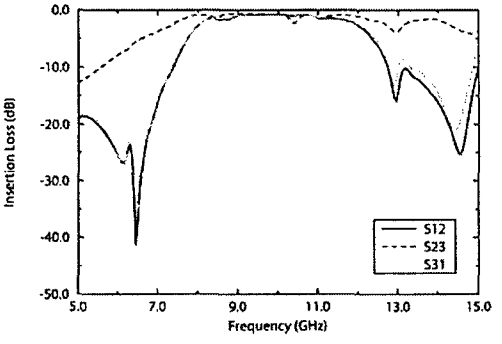

Figure 9

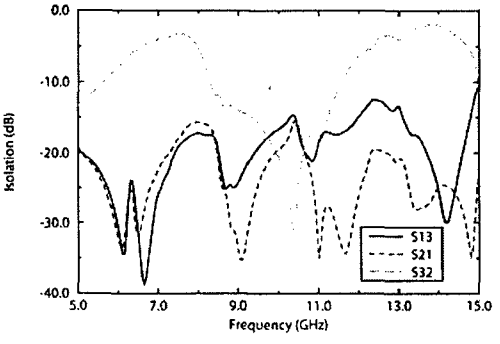

Figure 10

Figure 8 shows measured data of the return loss of all three ports. Note the marked difference in the measurements; port 1 exhibits narrower band performance compared to the other two ports. This difference is attributed to the high Q impedance data of Figure 6 verses the low Q impedance data of Figure 7. Figure 9 shows data associated with the three insertion loss measurements. This device exhibits moderately broad band performance for each of these three measurements, although the insertion loss between ports 2 and 3 is the broadest. Figure 10 shows measured isolation data. This plot is perhaps the most interesting, as two of the three measurements are quite broad band. Isolation between ports 2 and 1 is particularly broad, due in part to the low return loss in the stop-band. Using a 15 dB specification, the bandwidth is 10 GHz over the range from 5 to 15 GHz. While two of the isolation measurements exhibit very broad band performance, the third measurement presents a very narrow band response. In addition, the isolation data exhibits deep nulls of 30 dB or more in the pass-band. This suggests that the required load impedances are virtually the exact impedances for perfect isolation at specific frequencies. For all three ports in the 9 to 11 GHz band, the return loss is less than 15 dB, insertion loss is approximately 1 dB and isolation is less than 14 dB. Thus, for a 20% bandwidth, the square ferrite circulator can be used in many traditional applications.

A second design was fabricated using a circular ferrite puck in a microstrip transmission line configuration; see Figure 11. This device was fabricated on a Trans-Tech substrate of DA-9 (alumina, ε = 9.5) and with a ferrite material of Trans-Tech TT1-3000 ($4\pi M_s$= 3,000G, ε_f=12.9, $\tan\delta_f$ = 0.0005). The radius of the ferrite is 2.05mm and the dielectric thickness is 0.5mm. The coupling angle of the puck is 0.6 radians. The predicted wideband performance of this device is shown in Figure 13. Clearly the bandwidth performance of 6 to 15 GHz is exceptional with isolations and return losses not exceeding 20 dB and with insertion losses on the order of 0.5 dB.

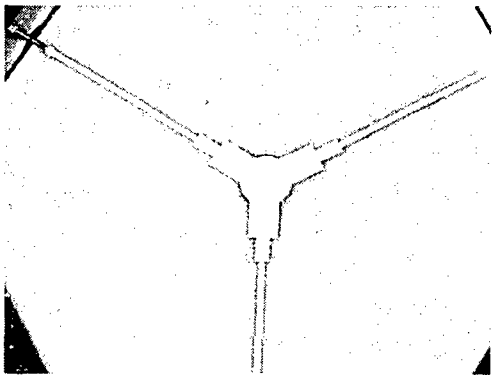

Figure 11

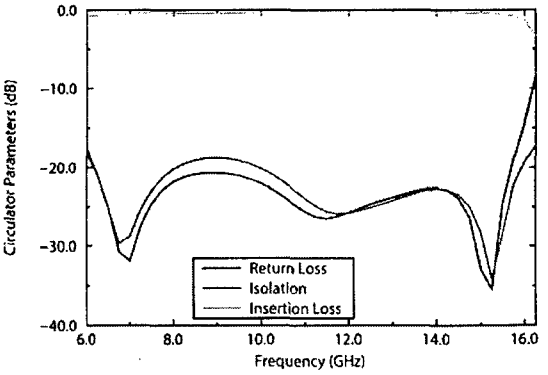

Figure 12

The previous device was fabricated, but the device operated very poorly. Upon making a hsyteresis loop measurement on the ferrite, the Group discovered that the vender used the wrong ferrite. The device will be re-fabricated and tested during Phase III.

Two activities associated with the experimental capability of the microwave group focused on the construction of a 5 meter, 2-40 GHz anechoic chamber and the construction of an FMR linewidth measurement system. The chamber's carcass was constructed, positioning equipment was installed, and instrumentation was acquired during Phase II; the absorbing material will be installed and data acquisition software will be written during Phase III. A photograph of the azimuth positioner in the carcass of the chamber is shown Figure 13.

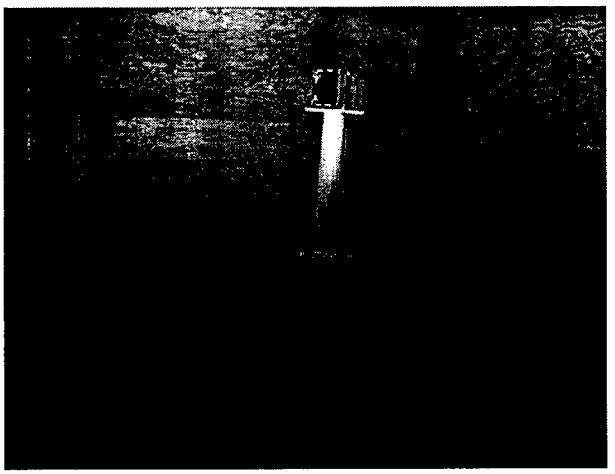

Figure 13

The FMR linewidth system was also configured and designed during Phase II. The data acquisition and control software was developed by Colorado State University, which serve as a subcontractor. Details about this system and preliminary test cases are supplied in Appendix C. A photograph of the University of Idaho's system is shown in Figure 14.

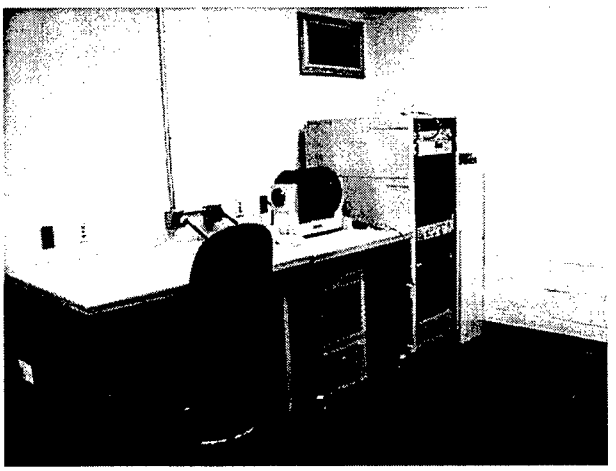

Figure 14

V. Future Work

As can be seen in the previous discussion, many activities have been initiated with the plans to bring them to fruition by the end of Phase III. With this in mind, preparations are under for:

- Experimentally characterize the best case loss of a ferrite puck. Use such experimental data to fabricate optimized circulators, particularly for self-bias applications.
- Develop numerical code that can accurately predict spin-wave effects in a microwave device (e.g., circulators).
- Finalize the development of the 2D waveguide model.
- Complete the construction of the anechoic chamber and the writing of the data acquisition software; prove-in the system.
- Complete and prove-in the FMR linewidth system

REPORT DOCUMENTATION PAGE

Form Approved
OMB No. 0704-0188

1. REPORT DATE *(DD-MM-YYYY)*	2. REPORT TYPE	3. DATES COVERED *(From - To)*
12/20/06	Final Technical Report	February 2005-December 2006

4. TITLE AND SUBTITLE
Advanced Microwave Ferrite Research (AMFeR): Phase Two

5a. CONTRACT NUMBER

5b. GRANT NUMBER
N00014-05-1-0239

5c. PROGRAM ELEMENT NUMBER

6. AUTHOR(S)
Jeffery L. Young

5d. PROJECT NUMBER

5e. TASK NUMBER

5f. WORK UNIT NUMBER

7. PERFORMING ORGANIZATION NAME(S) AND ADDRESS(ES)
University of Idaho
P.O. Box 443020
Moscow, ID 8384-3020

8. PERFORMING ORGANIZATION REPORT NUMBER

9. SPONSORING/MONITORING AGENCY NAME(S) AND ADDRESS(ES)
Dr. Colin Wood
Office of Naval Research
Code 312, Electronics Division
One Liberty Center
875 North Randolph Street, Suite 1425
Arlington, VA 22203-1995
703-696-4218
woodc@onr.navy.mil

10. SPONSOR/MONITOR'S ACRONYM(S)
ONR

11. SPONSORING/MONITORING AGENCY REPORT NUMBER
PR# 06PR05337-00

12. DISTRIBUTION AVAILABILITY STATEMENT
6.1 Basic Research; open for full circulation

13. SUPPLEMENTARY NOTES

14. ABSTRACT
Reported herein are the key findings and activities associated with the Office of Naval Research (ONR) Advance Microwave Ferrite Research (AMFeR) Phase Two project. This project was conceived to develop high anisotropy ferrite crystals for microwave, self-biased circulator devices. To date, barium-ferrite, c-axis crystals have been grown using several methods, including sputtering and liquid phase epitaxy, with the latter method being the most successful for the growth of thick crystals in excess of 100 microns. Micromagnetic simulations were carried out for various experimental films developed by the materials team. The microwave device team continued its investigation of the design of novel shaped ferrite microwave circulator and ferrite front-end microwave assemblies. Several microwave circulators were designed that achieved good isolation and bandwidth characteristics.

15. SUBJECT TERMS
circulators, ferrite, ferrite films, LPE, PLD, CVD, sputtering

16. SECURITY CLASSIFICATION OF:	17. LIMITATION OF ABSTRACT	18. NUMBER OF PAGES	19a. NAME OF RESPONSIBLE PERSON
			Jeffrey L. Young

INSTRUCTIONS FOR COMPLETING SF 298

a. REPORT	b. ABSTRACT	c. THIS PAGE	UU	47	19b. TELEPONE NUMBER (*Include area code*)
U	U	U			208-885-6829